To link to this article : DOI: 10.1016/j.combustflame.2013.11.014
http://dx.doi.org/10.1016/j.combustflame.2013.11.014

An analytical model for azimuthal thermoacoustic modes in an annular chamber fed by an annular plenum

Michaël Bauerheim [a,*], Jean-François Parmentier [a], Pablo Salas [b], Franck Nicoud [c], Thierry Poinsot [d]

[a] CERFACS, CFD team, 42 Av Coriolis, 31057 Toulouse, France
[b] INRIA Bordeaux – Sud Ouest, HiePACS Project, Joint INRIA-CERFACS Lab. on High Performance Computing, 33405 Talence, France
[c] Université Montpellier 2, I3M UMR CNRS 5149, Place E. Bataillon, 34095 Montpellier, France
[d] IMF Toulouse, INP de Toulouse and CNRS, 31400 Toulouse, France

A B S T R A C T

This study describes an analytical method for computing azimuthal modes due to flame/acoustics coupling in annular combustors. It is based on a quasi-one-dimensional zero-Mach-number formulation where *N* burners are connected to an upstream annular plenum and a downstream chamber. Flames are assumed to be compact and are modeled using identical flame transfer function for all burners, characterized by an amplitude and a phase shift. Manipulation of the corresponding acoustic equations leads to a simple methodology called ANR (annular network reduction). It makes it possible to retain only the useful information related to the azimuthal modes of the annular cavities. It yields a simple dispersion relation that can be solved numerically and makes it possible to construct coupling factors between the different cavities of the combustor. A fully analytical resolution can be performed in specific situations where coupling factors are small (weak coupling). A bifurcation appears at high coupling factors, leading to a frequency lock-in of the two annular cavities (strong coupling). This tool is applied to an academic case where four burners connect an annular plenum to a chamber. For this configuration, analytical results are compared with a full three-dimensional Helmholtz solver to validate the analytical model in both weak and strong coupling regimes. Results show that this simple analytical tool can predict modes in annular combustors and investigate strategies for controlling them.

Keywords:
Azimuthal modes
Analytical
Combustion instabilities
Coupling

1. Introduction

Describing the unstable acoustic modes that appear in annular gas turbine combustion chambers and finding methods to control them are the topic of multiple present research activities [1–9]. The complexity of these phenomena and the difficulty of performing simple laboratory-scale experiments explain why progress in this field has been slow for a long time since. Recently, the development of smaller annular chambers in laboratories has opened the path to investigating flow fields [10,11], ignition [12], flame response to acoustics [13], and azimuthal instabilities in these configurations [4,14,15]. At the same time, theoretical and numerical approaches have progressed in three directions: (1) full 3D LES of annular chambers has been developed [16,17], (2) 3D acoustic tools have been adapted to annular chambers [18–21], and (3) analytical approaches have been proposed to avoid the costs of 3D formulations and to investigate the stability and control of modes at low cost [5,22,23]. This last class of approaches is especially interesting for elucidating mechanisms (such as transverse forcing effect [23], symmetry breaking [5], and mode nature [24]) because they can provide explicit solutions for the frequency and the growth rate of all modes. The difficulty in these methods is in constructing a model that can be handled by simple analytical approaches while retaining most of the important physical phenomena and geometrical specificities of annular chambers.

One interesting issue in studies of instabilities in annular chambers is classifying them. For example, standing and turning modes [1,24] are both observed [1,5,17,25], but predicting which mode type will appear in practice and whether they can be studied and controlled with the same method remains difficult [23]. Similarly, most large-scale annular chambers exhibit multiple acoustic modes in the frequency range of interest (typically 10–30 acoustic modes can be identified in a large-scale industrial chamber between 0 and 300 Hz), and classifying them into categories is the first step in controlling them. These categories are typically "longitudinal vs azimuthal modes" or "modes involving only a part of the chamber (decoupled modes) vs modes involving the whole system (coupled modes)" [1,3,20,21]. Knowing that a given unstable mode is controlled only by a certain part of the combustor is an obvious asset for any control strategy. In the case of combustors including an annular plenum, burners, and an annular chamber,

* Corresponding author.
E-mail address: bauerheim@cerfacs.fr (M. Bauerheim).

Nomenclature

$\alpha = z_{f,i}/L_i$ normalized abscissa for the flame location in the burners
$\beta = \frac{c^0 L_p}{c_u^0 L_c}$ tuning parameter
ϵ_p and ϵ_c wavenumber perturbation in the plenum and chamber
$\Gamma_{i,k}$ kth coupling parameter of the ith sector
$\mathbb{F} = \frac{\rho^0 c^0}{\rho_u^0 c_u^0}(1 + n_i e^{j\omega\tau_i})$ flame parameter
ω angular frequency
ρ_u^0 and ρ^0 mean density in the unburnt and burnt gases
τ_i time delay of the FTF of the ith flame
$\tau_p^0 = \frac{2c_u^0}{pL_p}$ and $\tau_c^0 = \frac{2c^0}{pL_c}$ period of the unperturbed pth azimuthal mode of the plenum and chamber
θ angle in the annular cavities
c_u^0 and c^0 mean sound speed in the unburnt and burnt gases
k_u and k wavenumber in the unburnt and burnt gases
$L_c = \pi R_c$ and $L_p = \pi R_p$ half perimeter of the chamber or plenum
L_i length of the ith burner
N number of burners
n_i interaction index of the FTF of the ith flame
p order of the azimuthal mode
p' pressure fluctuations
R_c and R_p radii of the annular chamber or plenum
S_c, S_p, and S_i cross sections of the chamber, plenum, and ith burner
u' azimuthal velocity fluctuations (along x)
w' axial velocity fluctuations (along z)
x azimuthal abscissa in the chamber or plenum corresponding to $x_c = R_c\theta$ or $x_p = R_p\theta$
z longitudinal abscissa in the burners
ANR annular network reduction
ATACAMAC analytical tool to analyze and control azimuthal modes in annular combustors
BC burners + chamber configuration (Fig. 1 left)
BCp burner + chamber mode of order p (the annular plenum is perfectly decoupled from the system)
FDCp fully decoupled chamber mode of order p
FDPp fully decoupled plenum mode of order p
FTF flame transfer function
LES large eddy simulation
PBC plenum + burners + chamber configuration (Fig. 1 right)
PBp plenum + burner mode of order p (the annular chamber is perfectly decoupled from the system)
SCp strongly coupled mode of order p
WCCp weakly coupled chamber mode of order p
WCPp weakly coupled plenum mode of order p

such a classification is useful, for example, in understanding how azimuthal modes in the plenum and in the chamber (which have a different radius and sound speed and therefore different frequencies) can interact or live independently. For example, FEM simulations of a real industrial gas turbine [20] produce numerous complex modes that involve several cavities (plenum, burners, and chamber) at the same time. Unfortunately, determining whether certain parts of a chamber can be 'decoupled' from the rest of the chamber is a task for which there is no clear strategy. 'Decoupling' factors have been derived for longitudinal modes in academic burners where all modes are longitudinal [26]. Extending these approaches to annular systems requires first deriving analytical solutions that can isolate the effect of parameters on the modes structure. This is one of the objectives of this paper.

Noiray et al. [5] and Ghirardo and Juniper [23] have proposed analytical analysis of complex nonlinear mechanisms, but only in simple configurations where the combustor is modeled with an annular rig alone. Parmentier et al. [22] have derived an analytical method called ATACAMAC (for analytical tool to analyze and control azimuthal modes in annular combustors) for a more realistic configuration called BC (N burners + chamber) (Fig. 1 left). By describing acoustic wave propagation and flame action in a network of ducts representing the BC configuration and introducing a reduction method for the overall system corresponding to wave propagation in this network, they were able to predict the frequencies and growth rate of azimuthal and longitudinal modes, to identify their nature, and to predict their response to passive control methods such as symmetry breaking. Stow and Dowling [27] also investigated BC configurations with low-order models and focused on limit cycles by introducing more complex flame models (by adding nonlinearities and uniform spread of convection times).

However, BC geometries did not correspond exactly to real annular chambers where the N burners are connected not only downstream to the combustion chamber but also upstream to the plenum that feeds them. PBC configurations (plenum + N burners + chamber) (Fig. 1 right) have been proved [1,20] to correctly reproduce the behavior of complex industrial annular combustors (Fig. 2). Evesque and Polifke [8] studied PBC configurations using both FEM simulations and low-order models. Pankiewitz and Sattelmayer [21] also investigated this case using time-domain simulations with an axial mean flow. Both the linear and nonlinear flames regimes are studied by introducing saturations in the flame transfer functions. They pointed out that the time delay of the FTF plays a crucial role in predicting the frequency as well as the nature of azimuthal modes in such a configuration.

Thus, no full analytical resolution of the frequency and nature of azimuthal modes has been achieved in PBC configurations. The present paper extends the analytical methodology of Schuller et al. [26] for longitudinal tubes and of Parmentier et al. [22] for BC configurations to a PBC configuration with N burners in order to highlight key parameters involved in the coupling mechanisms.

In most network approaches to combustion instabilities, a very large matrix is built to describe the acoustics of the system [8,26,28]. Here, we introduce a significantly simpler methodology called ANR (annular network reduction) that makes it possible to reduce the size of the acoustic problem in an annular system to a simple 4-by-4 matrix containing all information of the combustor resonant modes. This method makes it possible to obtain explicit dispersion relations for PBC configurations and to exhibit the exact forms of the coupling parameters for azimuthal modes between the plenum and the burners, on one hand, and between the burners and the chamber, on the other hand.

The paper is organized as follows: Section 2 describes the principle of the ANR (annular network reduction) methodology and the submodels that account for active flames. The decomposition of the network into H-shaped connectors and azimuthal propagators makes it possible to build an explicit dispersion relation giving the frequency, growth rate, and structure of all modes. In Section 3, thermoacoustic regimes (from fully decoupled to strongly coupled) are defined, depending on the analytical coupling parameters conducted in Section 2. Finally, this analytical model is validated using the model annular chamber described in Section 4 with simplistic shapes to construct coupling factors and study azimuthal modes for a case where a plenum is connected to a chamber by four similar burners ($N = 4$). First the weakly coupled regime (Section 5) and then the strongly coupled regime (Section 6) are investigated.

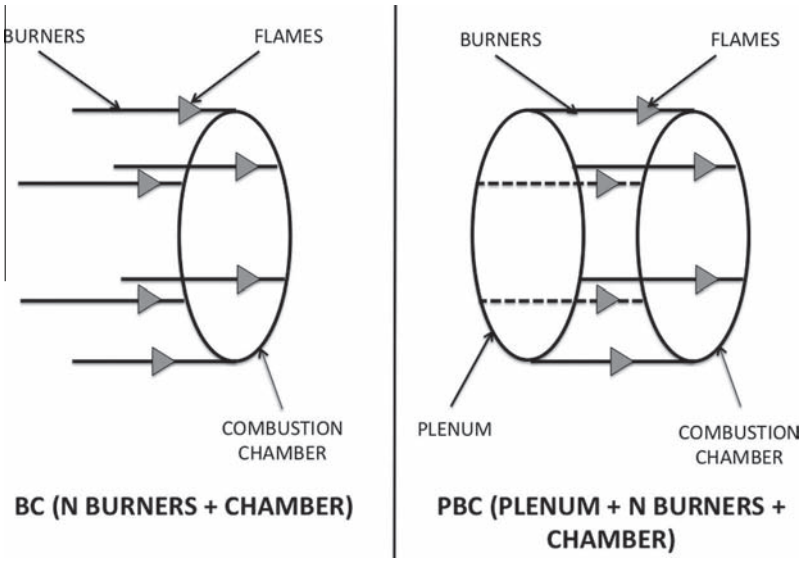

Fig. 1. Configurations for studying unstable modes in annular chambers.

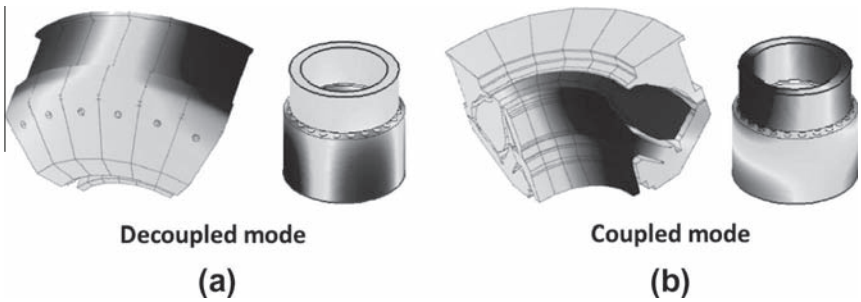

Fig. 2. FEM simulations performed by Campa et al. [20] on a complex industrial gas turbine (only six sectors are displayed) and its PBC configuration model. Two kinds of eigenmodes are observed: (a) decoupled mode and (b) coupled mode.

The bifurcation [29] from weakly to strongly coupled situations is triggered by increasing the flame interaction index controlling the flame response to the acoustic flow. Results show that ATACAMAC makes it possible to predict azimuthal turning and standing modes in a PBC configuration and performs as well as a 3D Helmholtz solver for all three regimes, while simple annular rigs [5,23] or BC models [22,27] are not able to capture the bifurcation from weakly to strongly coupled regimes.

2. A network model for PCB (plenum + burners + chamber) configurations

2.1. Model description

The model is based on a network view of the annular chamber fed by burners connected to an annular plenum (Fig. 3). This model is limited to situations where pressure fluctuations depend on the angle θ (or x) but not on z in the chamber and the plenum (they depend on the coordinate z only in the N burners). This case can be observed in combustors terminated in choked nozzles that behave almost like a rigid wall (i.e., $w' = 0$ under the low-upstream-Mach-number assumption [30]). Note, however, that this restriction prevents the present model from representing academic combustors where the combustion chamber is open to the atmosphere [4,14,15] and from predicting "mixed modes" appearing at higher frequencies in configurations terminated by choked nozzles [20].

Since the chamber inlet is also close to a velocity node, modes that have no variation along z can develop in the chamber, as shown by recent LES [31]. Radial modes (where p' depends on r) are neglected because they often occur at high frequency. Gas

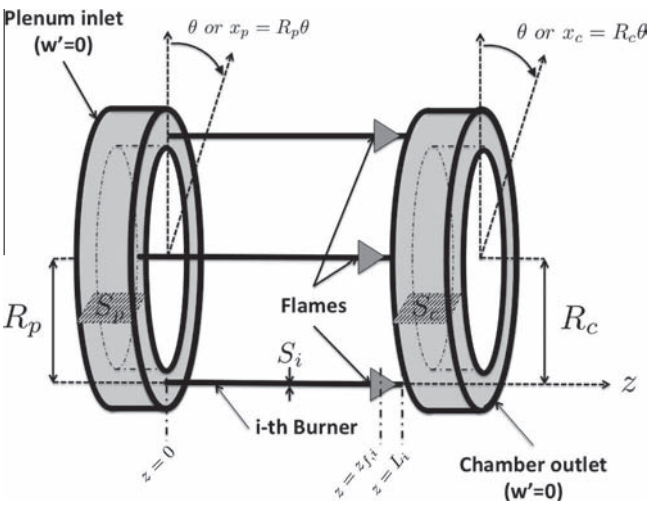

Fig. 3. Network representation of the plenum, burners, and chamber (PBC configuration).

dynamics is described using standard linearized acoustics for perfect gases in the low-Mach-number-approximation. The mean flow induced by swirlers remains slow [31], and azimuthal waves propagate at the sound speed, which is different in the plenum (fresh gas at sound speed c_u^0) and the chamber (burnt gas at sound speed c^0).

In the initial ATACAMAC study of Parmentier et al. [22], a BC (burners + chamber) configuration was considered: an annular chamber is fed by N burners without taking into account the existence of a plenum; the impedance imposed at the inlet of the N burners corresponded to a closed end ($w' = 0$), and flames were located at the burners, extremity ($z_{f,i} \simeq L_i$, where L_i is the length of the ith burner). This section describes how this BC case is extended to PBC (plenum + burners + chamber) configurations where an annular plenum feeds N ducts ("burners") that are all connected to an annular chamber. Most annular gas turbine chambers can be modeled using this scheme (Fig. 3).

In a PBC configuration, burners are connected at both ends to the annular plenum and chamber. The boundary conditions $w' = 0$ used for BC configurations are retained here only on walls of the annular cavities, not at the inlet/outlet sections of the burners. Mean density in the annular chamber is denoted ρ^0 (ρ_u^0 in the plenum). The subscript u stands for unburnt gases. The perimeter and the section of the annular plenum are denoted $2L_p = 2\pi R_p$ and S_p, respectively, while L_i and S_i stand for the length and cross-section area of the ith burner. The perimeter and the section of the annular chamber are denoted $2L_c = 2\pi R_c$ and S_c, respectively. The position along the annular plenum and chamber is given by the angle θ defining abscissa $x_p = R_p\theta$ for the plenum and $x_c = R_c\theta$ for the chamber. The location of the flames in the burners is given by the normalized abscissa $\alpha = z_{f,i}/L_i$ (Fig. 3).

2.2. Acoustic waves description and ANR methodology

To reduce the size of the system, a new methodology called ANR (annular network reduction) is proposed to extract only useful information on azimuthal modes of the resonant combustor. First, the combustor is decomposed into N sectors (Fig. 4) by assuming that every sector can be studied separately and that no flame-to-flame interaction occurs between neighboring sectors, a question that is still open today [32,33]. Staffelbach et al. [31] have shown that this was the case in LES of azimuthal modes. Worth and Dawson [4,34] have also demonstrated experimentally that this assumption in annular combustors is valid when the distance between burners is large enough to avoid flames merging.

For each individual sector, the acoustic problem may be split into two parts: propagation (Section 2.2.1 and already described in [22,35,36]) and H-shaped connector (Section 2.2.2) (Fig. 5).

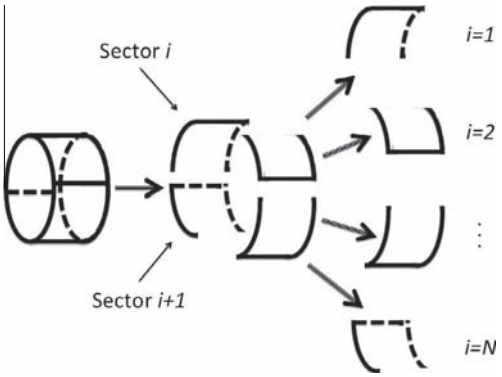

Fig. 4. Decomposition of an annular combustor into N sectors.

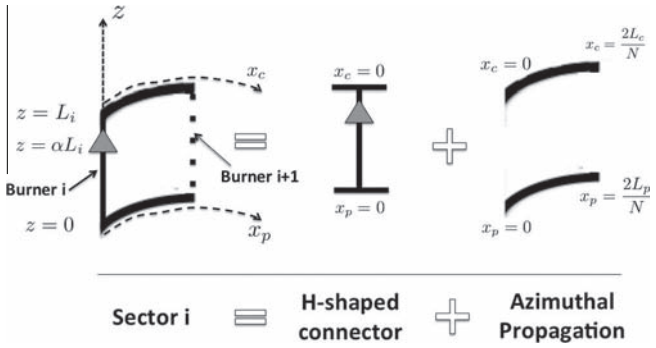

Fig. 5. ANR methodology: splitting of one sector into propagation and H-shaped section parts for a PBC configuration.

The angle θ and the coordinates of the plenum x_p and chamber x_c take their origin at the burner i. The end of the sector i is located at $x_p = \frac{2L_p}{N}$ and $x_c = \frac{2L_c}{N}$ (thus assuming that burners are evenly located around the annular combustor). H-shaped connectors are assumed to be compact regarding the acoustic wavelength.

2.2.1. Propagation

There are two main paths to analyzing azimuthal modes in annular chambers with simple models. The first is to write the mode explicitly as a function of the azimuthal angle θ, as done in [7,8], for example. The second approach is to use a network discretization along the azimuthal direction [1,22]. An advantage of the first method is the capability of considering modes that are azimuthal but also involve an axial dependance, something that cannot be done yet with the second approach. However, the second method describes explicitly the coupling between annular cavities and burners and therefore has been applied here for ATACAMAC.

Assuming linear acoustics, the pressure and velocity perturbations inside the ith sector of the annular chamber (denoted via subscript c,i) can be written as

$$p'_{c,i}(x_c,t) = (A_i\cos(kx_c) + B_i\sin(kx_c))e^{-j\omega t}, \tag{1}$$

$$\rho^0 c^0 u'_{c,i}(x_c,t) = j(A_i\sin(kx_c) - B_i\cos(kx_c))e^{-j\omega t}, \tag{2}$$

where $j^2 = -1$, $k = \omega/c^0$ is the wavenumber, and A_i and B_i are complex constants.

From Eqs. (1) and (2), pressure and velocity perturbations at two positions in the chamber x_{c0} and $x_{c0} + \Delta x_c$ are linked by

$$\begin{bmatrix} p'_{c,i} \\ \frac{1}{j}\rho^0 c^0 u'_{c,i} \end{bmatrix}_{(x_{c0}+\Delta x_c,t)} = \underbrace{\begin{bmatrix} \cos(k\Delta x_c) & -\sin(k\Delta x_c) \\ \sin(k\Delta x_c) & \cos(k\Delta x_c) \end{bmatrix}}_{R(k\Delta x_c)} \begin{bmatrix} p'_{c,i} \\ \frac{1}{j}\rho^0 c^0 u'_{c,i} \end{bmatrix}_{(x_{c0},t)}. \tag{3}$$

The matrix $R(k\Delta x_c)$ is a 2D rotation matrix of angle $k\Delta x_c$. In the case where N burners are equally distributed over the annular chamber, the propagation in the chamber between burners is fully described by the transfer matrix $R(k\frac{2L_c}{N})$, where $2L_c$ is the chamber perimeter.

Wave propagation in the ith sector of the plenum satisfies the same equation as in the chamber if the sound speed in fresh gases c_u^0 is used,

$$\begin{bmatrix} p'_{p,i} \\ \frac{1}{j}\rho_u^0 c_u^0 u'_{p,i} \end{bmatrix}_{(x_0+\Delta x_p,t)} = \underbrace{\begin{bmatrix} \cos(k_u\Delta x_p) & -\sin(k_u\Delta x_p) \\ \sin(k_u\Delta x_p) & \cos(k_u\Delta x_p) \end{bmatrix}}_{R(k_u\Delta x_p)} \begin{bmatrix} p'_{p,i} \\ \frac{1}{j}\rho_u^0 c_u^0 u'_{p,i} \end{bmatrix}_{(x_0,t)}, \tag{4}$$

where $k_u = \omega/c_u^0$.

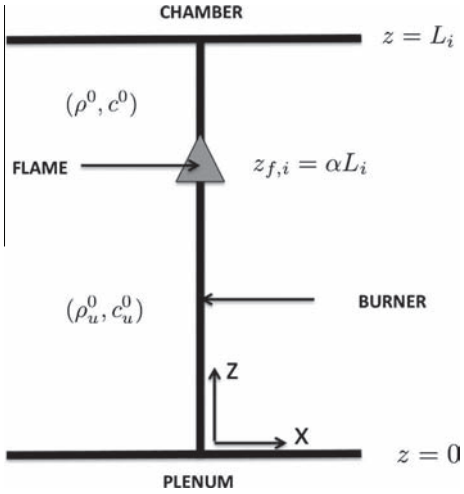

Fig. 6. Propagation in the ith burner for a PBC configuration in the ANR method.

Propagation in the ith burner from the plenum ($z = 0$) to the flame ($z = \alpha L_i$) and from $z = \alpha L_i$ to $z = L_i$ (Fig. 6) can be described in the same way, assuming propagation in fresh gases for the first part ($0 < z < \alpha L_i$) and in hot gases in the second part ($\alpha L_i < z < L_i$):

Therefore, equations for wave propagation in the ith burner are

$$\begin{bmatrix} p'_i \\ \frac{1}{j}\rho_u^0 c_u^0 w'_i \end{bmatrix}_{(\alpha L_i, t)} = R(k_u \alpha L_i) \begin{bmatrix} p'_i \\ \frac{1}{j}\rho_u^0 c_u^0 w'_i \end{bmatrix}_{(0,t)} \tag{5}$$

and

$$\begin{bmatrix} p'_i \\ \frac{1}{j}\rho^0 c^0 w'_i \end{bmatrix}_{(L_i, t)} = R(k(1-\alpha)L_i) \begin{bmatrix} p'_i \\ \frac{1}{j}\rho^0 c^0 w'_i \end{bmatrix}_{(\alpha L_i, t)}. \tag{6}$$

2.2.2. H-shaped connector

The physical parameters at the entrance (located at the end of the $(i-1)$th sector corresponding to $\theta = \frac{2\pi}{N}$ and consequently $x_p = \frac{2L_p}{N}$ and $x_c = \frac{2L_c}{N}$) must be linked to the output parameters (corresponding to the beginning of the ith sector located at $\theta = 0$ and consequently $x_p = x_c = 0$), as shown in Fig. 7.

The H-shaped connectors are treated as compact elements in the azimuthal direction. Jump conditions are first written along the x direction at $z = 0$ and $z = L_i$: at low Mach number [2], they correspond to the continuity of pressure and volume rate through the interface. For the sake of simplicity, more complex interactions (e.g., effective length or pressure drop effects) [20] are neglected, knowing they could affect the coupling mechanisms between cavities. At $z = L_i$,

$$p'_{c,i-1}\left(x_c = \frac{2L_c}{N}, t\right) = p'_{c,i}(x_c = 0, t) = p'_i(z = L_i), \tag{7}$$

$$S_c u'_{c,i-1}\left(x_c = \frac{2L_c}{N}, t\right) + S_i w'_i(z = L_i) = S_c u'_{c,i}(x_c = 0, t), \tag{8}$$

and at $z = 0$,

$$p'_{p,i-1}\left(x_p = \frac{2L_p}{N}, t\right) = p'_{p,i}(x_p = 0, t) = p'_i(z = 0), \tag{9}$$

$$S_p u'_{p,i-1}\left(x_p = \frac{2L_p}{N}, t\right) = S_i w'_i(z = 0) + S_p u'_{p,i}(x_p = 0, t). \tag{10}$$

Jump conditions are also required in the burners through the flames located at $z = z_{f,i}$. They are assumed to be planar and compact: their thickness is negligible compared to the acoustic wavelength. Flames are located at $z = z_{f,i}^+ = z_{f,i}^- \simeq \alpha L_i$, where superscripts + and − denote the downstream and upstream positions of the ith flame. At low Mach number, jump conditions through the flame imply equality of pressure and flow rate discontinuity due to an extra volume source term related to unsteady combustion [2],

$$p'_i\left(z_{f,i}^+\right) = p'_i\left(z_{f,i}^-\right), \tag{11}$$

$$S_i w'_i\left(z_{f,i}^+\right) = S_i w'_i\left(z_{f,i}^-\right) + \frac{\gamma_u - 1}{\gamma_u P^0}\dot{\Omega}'_{T,i}, \tag{12}$$

where P^0 is the mean pressure and γ_u is the heat capacity ratio of fresh gases. The unsteady heat release $\dot{\Omega}'_{T,i}$ is expressed using the FTF model (flame transfer function) [37],

$$\frac{\gamma_u - 1}{\gamma_u P^0}\dot{\Omega}'_{T,i} = S_i n_i e^{j\omega\tau_i} w'_i\left(z_{f,i}^-\right), \tag{13}$$

where the interaction index n_i[1] and the time delay τ_i are input data (depending on frequency) describing the interaction of the ith flame with acoustics. Therefore, the jump condition in Eq. (12) is recast using Eq. (13):

$$S_i w'_i\left(z_{f,i}^+\right) = S_i(1 + n_i e^{j\omega\tau_i}) w'_i\left(z_{f,i}^-\right). \tag{14}$$

Thanks to Eqs. (7)–(14), a transfer matrix T_i of the H-shaped connector of Fig. 7 is defined as

$$\begin{bmatrix} p'_p(x_p = 0, t) \\ \frac{1}{j}\rho_u^0 c_u^0 u'_p(x_p = 0, t) \\ p'_c(x_c = 0, t) \\ \frac{1}{j}\rho^0 c^0 u'_c(x_c = 0, t) \end{bmatrix}_i = T_i \begin{bmatrix} p'_p(x_p = \frac{2L_p}{N}, t) \\ \frac{1}{j}\rho_u^0 c_u^0 u'_p\left(x_p = \frac{2L_p}{N}, t\right) \\ p'_c(x_c = \frac{2L_c}{N}, t) \\ \frac{1}{j}\rho^0 c^0 u'_c(x_c = \frac{2L_c}{N}, t) \end{bmatrix}_{i-1}, \tag{15}$$

where the transfer matrix T_i is

$$T_i = I_d + 2\begin{bmatrix} 0 & 0 & 0 & 0 \\ \Gamma_{i,1} & 0 & \Gamma_{i,2} & 0 \\ 0 & 0 & 0 & 0 \\ \Gamma_{i,3} & 0 & \Gamma_{i,4} & 0 \end{bmatrix} \tag{16}$$

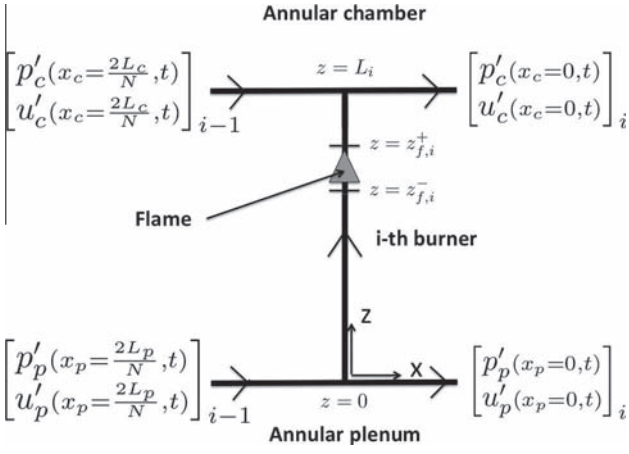

Fig. 7. H-shaped overview in the ANR method.

[1] Typical values of the interaction index n_i can reach $T_b/T_u - 1$ at low frequency.

and the coefficients $\Gamma_{i,k}$, $k = 1$—4, are

$$\Gamma_{i,1} = -\frac{1}{2}\frac{S_i}{S_p}\frac{\cos(k(1-\alpha)L_i)\cos(k_u\alpha L_i) - \mathbb{F}\sin(k(1-\alpha)L_i)\sin(k_u\alpha L_i)}{\cos(k(1-\alpha)L_i)\sin(k_u\alpha L_i) + \mathbb{F}\sin(k(1-\alpha)L_i)\cos(k_u\alpha L_i)}, \tag{17}$$

$$\Gamma_{i,2} = \frac{1}{2}\frac{S_i}{S_p}\frac{1}{\cos(k(1-\alpha)L_i)\sin(k_u\alpha L_i) + \mathbb{F}\sin(k(1-\alpha)L_i)\cos(k_u\alpha L_i)}, \tag{18}$$

$$\Gamma_{i,3} = \frac{1}{2}\frac{S_i}{S_c}\frac{\mathbb{F}}{\cos(k(1-\alpha)L_i)\sin(k_u\alpha L_i) + \mathbb{F}\sin(k(1-\alpha)L_i)\cos(k_u\alpha L_i)}, \tag{19}$$

$$\Gamma_{i,4} = -\frac{1}{2}\frac{S_i}{S_c}\frac{\mathbb{F}\cos(k(1-\alpha)L_i)\cos(k_u\alpha L_i) - \sin(k(1-\alpha)L_i)\sin(k_u\alpha L_i)}{\cos(k(1-\alpha)L_i)\sin(k_u\alpha L_i) + \mathbb{F}\sin(k(1-\alpha)L_i)\cos(k_u\alpha L_i)}, \tag{20}$$

with the flame parameter $\mathbb{F}$:

$$\mathbb{F} = \frac{\rho^0 c^0}{\rho_u^0 c_u^0}(1 + ne^{j\omega\tau}). \tag{21}$$

These coefficients are the coupling parameters for PBC configurations. $\Gamma_{i,1}$ and $\Gamma_{i,2}$ are linked to the plenum/burner junction (depending on S_i/S_p, which measures the ratio between the burner section S_i and the plenum section S_p), while $\Gamma_{i,3}$ and $\Gamma_{i,4}$ are linked to the chamber/burner junction (depending on S_i/S_c, which measures the ratio of the burner section to the chamber section (Fig. 3)).

2.3. Dispersion relation calculation given by the ANR method

In previous sections, the overall problem has been split into smaller parts, and now it has to be reconstructed to obtain the dispersion relation for the whole system. First, the pressure and velocity fluctuations at the end of the $(i-1)$th sector are linked to those at the end of the ith sector using Eqs. (3), (4), and (15),

$$\begin{aligned}\begin{bmatrix} p'_p\left(x_p = \frac{2L_p}{N}, t\right) \\ \frac{1}{j}\rho_u^0 c_u^0 u'_p\left(x_p = \frac{2L_p}{N}, t\right) \\ p'_c(x_c = \frac{2L_c}{N}, t) \\ \frac{1}{j}\rho^0 c^0 u'_c(x_c = \frac{2L_c}{N}, t) \end{bmatrix}_i &= R_i \begin{bmatrix} p'_p(x_p = 0, t) \\ \frac{1}{j}\rho_u^0 c_u^0 u'_p(x_p = 0, t) \\ p'_c(x_c = 0, t) \\ \frac{1}{j}\rho^0 c^0 u'_c(x_c = 0, t) \end{bmatrix}_i \\ &= R_i T_i \begin{bmatrix} p'_p\left(x_p = \frac{2L_p}{N}, t\right) \\ \frac{1}{j}\rho_u^0 c_u^0 u'_p(x_p = \frac{2L_p}{N}, t) \\ p'_c(x_c = \frac{2L_c}{N}, t) \\ \frac{1}{j}\rho^0 c^0 u'_c(x_c = \frac{2L_c}{N}, t) \end{bmatrix}_{i-1},\end{aligned} \tag{22}$$

where T_i is the matrix defined in Eq. (16) and R_i is the propagation matrix inside the plenum and chamber in the ith sector, defined by

$$R_i = \begin{bmatrix} R\left(k_u\frac{2L_p}{N}\right) & \begin{matrix} 0 & 0 \\ 0 & 0 \end{matrix} \\ \begin{matrix} 0 & 0 \\ 0 & 0 \end{matrix} & R\left(k\frac{2L_c}{N}\right) \end{bmatrix}, \tag{23}$$

where $R\left(k_u\frac{2L_p}{N}\right)$ and $R\left(k\frac{2L_c}{N}\right)$ are 2-by-2 matrices defined in Eqs. (3) and (4)

Then Eq. (22) can be repeated through the N sectors, and periodicity imposes that

$$\begin{bmatrix} p'_p\left(x_p = \frac{2L_p}{N}, t\right) \\ \frac{1}{j}\rho_u^0 c_u^0 u'_p\left(x_p = \frac{2L_p}{N}, t\right) \\ p'_c(x_c = \frac{2L_c}{N}, t) \\ \frac{1}{j}\rho^0 c^0 u'_c(x_c = \frac{2L_c}{N}, t) \end{bmatrix}_{i=1} = \left(\prod_{i=N}^{1} R_i T_i\right) \begin{bmatrix} p'_p\left(x_p = \frac{2L_p}{N}, t\right) \\ \frac{1}{j}\rho_u^0 c_u^0 u'_p\left(x_p = \frac{2L_p}{N}, t\right) \\ p'_c(x_c = \frac{2L_c}{N}, t) \\ \frac{1}{j}\rho^0 c^0 u'_c(x_c = \frac{2L_c}{N}, t) \end{bmatrix}_{i=1}. \tag{24}$$

System Eq. (24) leads to non-null solutions if and only if its determinant is null,

$$\det\left(\prod_{i=N}^{1} R_i T_i - I_d\right) = 0, \tag{25}$$

where I_d is the 4-by-4 identity matrix and the matrix $M = \prod_{i=N}^{1} R_i T_i$ is the transfer matrix of the overall system. Eq. (25) provides an implicit equation for the pulsation ω and gives the stability limits and the frequency of unstable modes. Note that Eq. (25) given by the ANR methodology only involves a 4-by-4 determinant[2] irrespective of the number of burners N.

3. Analytical procedure and coupling limits

Due to significant nonlinearities, Eq. (25) cannot be solved analytically in the general case. However, different situations (Fig. 8) can be exhibited where Eq. (25) can be solved, depending on values taken by the coupling parameters $\wp_{p,i}$ and $\wp_{c,i}$:

$$\wp_{p,i} = \max(|\Gamma_{i,1}|, |\Gamma_{i,2}|) \tag{26}$$

and

$$\wp_{c,i} = \max(|\Gamma_{i,3}|, |\Gamma_{i,4}|). \tag{27}$$

The parameters $\wp_{p,i}$ and $\wp_{c,i}$ measure the coupling effect of the plenum/burner junction and the chamber/burner junction, respectively, for the ith sector. They depend only on the geometry (section ratios S_i/S_p and S_i/S_c as well as the burner's length L_i) and the flame (the flame interaction factor $\mathbb{F}$ and the flame position α). Longitudinal modes in the burners can be obtained with this model, but only purely azimuthal modes will be studied in this paper (Fig. 8).

3.1. Fully decoupled situations (FDPp and FDCp)

If the coupling parameters have vanishing small values ($\wp_{p,i} = 0$ and $\wp_{c,i} = 0$), the coupling matrices of each sector (T_i in Eq. (25)) are the identity matrix. As a consequence, the dispersion relation (Eq. (25)) reduces to

$$\det\left(\prod_{i=N}^{1} R_i - I_d\right) = 0. \tag{28}$$

The matrices R_i being block matrices of 2-by-2 rotation matrices that satisfy $R(\theta_1)R(\theta_2) = R(\theta_1 + \theta_2)$, Eq. (28) becomes

$$\begin{aligned}\det\left(\prod_{i=N}^{1} R_i - I_d\right) &= \det\left(\begin{bmatrix} R(2k_uL_p) - I_d & \begin{matrix} 0 & 0 \\ 0 & 0 \end{matrix} \\ \begin{matrix} 0 & 0 \\ 0 & 0 \end{matrix} & R(2kL_c - I_d) \end{bmatrix}\right) \\ &= \det(R(2k_uL_p) - I_d)\det(R(2kL_c) - I_d) = 0.\end{aligned} \tag{29}$$

[2] The ANR methodology retains only useful information related to azimuthal modes of the annular cavities. Knowing that these modes are a combination of two characteristic waves, the minimum size of the matrix system is $2\mathcal{C}$-by-$2\mathcal{C}$, where $\mathcal{C}$ is the number of annular cavities (here $\mathcal{C} = 2$: plenum + chamber).

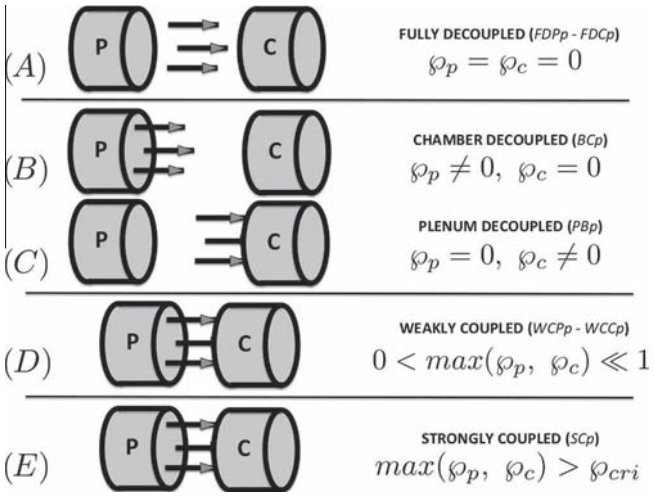

Fig. 8. The four coupling situations depending on the parameters $\wp_p$ and $\wp_c$.

Solutions of Eq. (29) are $k_u L_p = p\pi$ and $kL_c = p\pi$, where p is an integer. They correspond to two families of modes that live separately (case A in Fig. 8):

- **FDPp—fully decoupled plenum mode of order *p***: They satisfy the relation $k_u L_p = p\pi$ and correspond to the azimuthal modes of the annular plenum alone (Fig. 8).
- **FDCp—fully decoupled chamber mode of order *p***: They satisfy the relation $kL_c = p\pi$ and correspond to the azimuthal modes of the annular chamber alone (Fig. 8).

3.2. Chamber or plenum decoupled situations (PBp and BCp)

These situations correspond to cases where either the plenum or the chamber is fully decoupled from the burners, i.e., respectively $\wp_p = 0$ or $\wp_c = 0$, (cases B and C in Fig. 8). The transfer matrices of each sector are block-triangular, leading to a simple relation for the determinant and consequently for the dispersion relation (Eq. (25)) without assumption on the non-null parameter $\wp_p$ or $\wp_c$. As for the fully decoupled situations, two families of modes can be exhibited (cases B and C in Fig. 8):

- **PBp—plenum/burners mode of order *p*:** In this situation, $\wp_c = 0$. The annular chamber is fully decoupled from the system (burners + plenum) and the dispersion relation Eq. (25) reduces to two equations:

$$\det(R(2kL_c) - 1) = 0 \tag{30}$$

$$\det\left(\prod_{i=N}^{1} R\left(\frac{2k_u L_p}{N}\right)\begin{bmatrix} 1 & 0 \\ \Gamma_{i,1} & 1 \end{bmatrix} - I_d\right) = 0. \tag{31}$$

Eq. (30) corresponds to the dispersion relation of a FDCp mode, while Eq. (31) is the dispersion relation of a PB (plenum + burners) configuration where an impedance $Z = 0$ is imposed at the downstream end of the burner, simulating the large chamber decoupled from the system (case B in Fig. 8). This latter mode is referred to as "PBp" standing for plenum/burners mode of order p. These situations are, however, unrealistic because they neglect all interactions between the annular plenum and chamber: the only solution to obtaining $\wp_c \to 0$ in a PBC configuration is an infinite cross section of the chamber ($S_c \to \infty$ in Eqs. (19) and (20)). Therefore, this paper will focus on other situations (e.g., cases D and E in Fig. 8) that are more representative of real engines by including the interaction between annular cavities.

- **BCp—burners/chamber mode of order *p*:** In this situation, $\wp_p = 0$, so the annular plenum is fully decoupled from the rest of the system and the dispersion relation Eq. (25) reduces to two equations:

$$\det(R(2k_u L_p) - 1) = 0 \tag{32}$$

$$\det\left(\prod_{i=N}^{1} R\left(\frac{2kL_c}{N}\right)\begin{bmatrix} 1 & 0 \\ \Gamma_{i,4} & 1 \end{bmatrix} - I_d\right) = 0. \tag{33}$$

The first equation (Eq. (32)) is the dispersion relation of a FDPp mode, while Eq. (33) is the dispersion relation of a BC (burners + chamber) configuration where a pressure node ($Z = 0$) is imposed at the upstream end of the burner, modeling the large plenum decoupled from the burners and the annular chamber (case C in Fig. 8). This latter mode is called "BCp" for burners/chamber mode of order p and was already studied by Parmentier et al. [22].

3.3. Weakly coupled situations (WCPp and WCCp)

When $\wp_p$ and $\wp_c$ are both nonzero, both azimuthal modes of the plenum and the chamber can exist and interact through the burners. If $\wp_p$ and $\wp_c$ remain small (Eq. (34)), an asymptotic solution can be constructed:

$$\forall i, \quad 0 < \wp_{p,i} \ll 1 \quad \text{and} \quad 0 < \wp_{c,i} \ll 1. \tag{34}$$

The parameters $\wp_{p,i}$ (Eq. (26)) and $\wp_{c,i}$ (Eq. (27)) measure the strength of the coupling effect of the plenum/burner junction and the chamber/burner junction, respectively, for the ith sector. If they are small, the transfer matrices of each sector ($T_i R_i$ in Eq. (25)) are close to the rotation matrix R_i defined in Eq. (4), so that the eigenfrequencies of the system will be close to a FDPp or a FDCp mode. Consequently, as for fully decoupled modes, two families of modes can be exhibited (case D in Fig. 8):

- **WCPp—weakly coupled plenum mode of order *p*:** This mode is close to a FDPp mode, and the solution for the wavenumber k_u can be searched for as an expansion around this case,

$$k_u L_p = p\pi + \epsilon_p, \tag{35}$$

where $\epsilon_p \ll p\pi$.
- **WCCp—weakly coupled chamber mode of order *p*:** This mode is close to a FDCp mode, and the solution for the wavenumber k can be searched for as an expansion around this case,

$$kL_c = p\pi + \epsilon_c, \tag{36}$$

where $\epsilon_c \ll p\pi$.

For weakly coupled modes, this low-coupling assumption allows a Taylor expansion of the dispersion relation (Eq. (25)), which can be truncated and solved, providing analytical solutions for ϵ_c and ϵ_p. This expansion is case-dependent: The $N = 4$ case will be detailed in Section 5. Basically, results show that azimuthal modes will be either chamber or plenum modes slightly modified by their interaction with the rest of the combustor.

Note that the low-coupling assumption ($\wp_{p,i} \ll 1$ and $\wp_{c,i} \ll 1$) does not imply low thermoacoustic coupling ($n_i \ll 1$) because surface ratios between burner and plenum or chamber are usually small ($S_i/S_c \ll 1$ and $S_i/S_p \ll 1$).

In the specific configuration where the flames are located at the end of the burner ($\alpha = z_{f,i}/L_i = 1$ in Fig. 3), however, the coupling parameters simplify as

$$\Gamma_{i,1} = -\frac{1}{2}\frac{S_i}{S_p}\,\mathrm{cotan}(k_u L_i), \tag{37}$$

$$\Gamma_{i,2} = \frac{1}{2}\frac{S_i}{S_p}\frac{1}{\sin(k_u L_i)}, \tag{38}$$

$$\Gamma_{i,3} = \frac{1}{2}\frac{S_i}{S_c}\frac{\mathbb{F}}{\sin(k_u L_i)}, \tag{39}$$

$$\Gamma_{i,4} = -\frac{1}{2}\frac{S_i}{S_c}\mathbb{F}\,\mathrm{cotan}(k_u L_i), \tag{40}$$

where $\mathbb{F}$ is the flame parameter defined in Eq. (21). Eqs. (37)–(40) correspond to an extension of the coupling parameters proposed by Schuller et al. [26] for longitudinal instabilities and Parmentier et al. [22] for azimuthal instabilities in a BC configuration. They show that decoupling ($\wp_{p,i} \ll 1$ and $\wp_{c,i} \ll 1$) can be expected in this case for small section ratios $S_i/S_p \ll 1$ and $S_i/S_c \ll 1$, when the flame parameter $\mathbb{F}$ (Eq. (21)) is small too.

3.4. Strongly coupled situations (SCp)

The low-coupling assumption ($\wp_{p,i} \ll 1$ and $\wp_{c,i} \ll 1$) is not valid at high flame-interaction factors $\left(\mathbb{F} = \frac{\rho^0 c^0}{\rho_u^0 c_u^0}(1 + ne^{j\omega\tau})\right)$ or high surface ratios (S_i/S_p or S_i/S_c). In these situations (case E in Fig. 8), a numerical resolution of the analytical dispersion relation (Eq. (25)) is required. It can be achieved by a nonlinear solver based on the Newton–Raphson algorithm.

No rule already exists to distinguish a weakly or strongly coupled situation for real engines (characterized by an unknown critical parameter $\wp_{crit}$, Fig. 8). Moreover, classifying modes into two families, as is the case for fully decoupled situations (FDPp and FDCp modes), plenum or chamber decoupled situations (PBp and BCp modes), and weakly decoupled situations (WCPp and WCCp modes), is not possible any more due to the interaction between all parts of the system. A first attempt to identify key parameters and rules to differentiate weakly and strongly coupled situations is described in Section 6.

In the remaining of the paper, the weakly and strongly coupled situations (Fig. 8) will be studied in the PBC configuration with four burners ($N = 4$) described in Section 4. The transition from weakly (Section 5) to strongly coupled (Section 6) regimes is controlled by a critical coupling limit factor $\wp_{crit}$. The transition occurs when $\max(\wp_p, \wp_c) > \wp_{\mathrm{crit}}$. The geometry being fixed (Table 1) and the coupling parameters ($\wp_p$ and $\wp_c$) depending only on the geometry and the flame, the transition will be triggered by increasing the flame interaction index n_i of the flames from $n_i = 1.57$ (weak coupling) to $n_i = 8.0$ (strong coupling).

Table 1
Parameters used for numerical applications.

Chamber			
Half perimeter	L_c	6.59	m
Section	S_c	0.6	m^2
Plenum			
Half perimeter	L_p	6.59	m
Section	S_p	0.6	m^2
Burner			
Length	L_i^0	0.6	m
Section	S_i	0.03	m^2
Fresh gases			
Mean pressure	p^0	2×10^6	Pa
Mean temperature	T_u^0	700	K
Mean density	ρ_u^0	9.79	kg/m^3
Mean sound speed	c_u^0	743	m/s
Burnt gases			
Mean pressure	p^0	2×10^6	Pa
Mean temperature	T^0	1800	K
Mean density	ρ^0	3.81	kg/m^3
Mean sound speed	c^0	1191	m/s
Flame parameters			
Interaction index	n_i	Variable	–
Time delay	τ_i	Variable	s
Thickness	e_{fl}	0.03	m

Note: Parameters correspond to a typical large-scale industrial gas turbine.

4. Validation in a simplified model chamber

Eigenfrequencies and mode structures of the analytical resolution of the dispersion relation under the low-coupling-factors assumption (Fig. 8, all modes except SCp) are first compared to a full 3D acoustic code and to the direct resolution of Eq. (25) in the case of a simplified 3D PBC configuration, which is used as a toy model for ATACAMAC and corresponds to a typical industrial gas turbine.

4.1. Description of the simplified PBC configuration

The 3D geometry (Fig. 9) corresponds to a PBC setup with $N = 4$ burners, similar to Fig. 3 (characteristics defined in Table 1). The mean radii R_p and R_c of the cylindrical chamber and plenum are derived from the half perimeter L_p and L_c of the analytical model. Boundary conditions correspond to impermeable walls everywhere.

4.2. Description of the 3D acoustic code

To validate the assumptions used in the ATACAMAC formulation, it is interesting to compare its results with the output of a full 3D acoustic solver. Here, AVSP was used. AVSP is a parallel 3D code devoted to the resolution of acoustic modes of industrial combustion chambers [38]. It solves the eigenvalues problem issued from a discretization on unstructured meshes of the Helmholtz equation with a source term due to the flames. The mesh used here (Fig. 9, left) is composed of 230,000 cells, which ensures grid independence. The flame–acoustic interaction is taken into account via the FTF model [37] similarly to the expression used in Eq. (13). The local reaction term is expressed in burner i as

$$\dot{\omega}_i = n_{u,i} e^{j\omega\tau_i} w'(\mathbf{x}_{\mathrm{ref},i}). \tag{41}$$

The local interaction index $n_{u,i}$ describes the local flame–acoustic interactions. The values of $n_{u,i}$ are assumed to be constant in the flame zone i (Fig. 9) and are chosen to recover the global value of interaction index n_i of the infinitely thin flame when integrated over the flame zone i [38]. They are also assumed to be independent of frequency for simplicity. Heat release fluctuations in each flame zone are driven by the velocity fluctuations at the reference points $\mathbf{x}_{\mathrm{ref},i}$ located in the corresponding burner. In the infinitely thin flame model these reference points are the same as the flame locations z_f. In AVSP, the reference points were placed a few millimeters upstream of the flames (Fig. 9) to avoid numerical issues. This was proved to have only a marginal effect on the computed frequency [38,39].

4.3. Construction of a quasi-1D network from a real 3D combustor

A quasi-one-dimensional model of a simplified PBC configuration described in Section 4.1 can be constructed using Table 1. Even though the present model is quasi-one-dimensional, simple corrections can be incorporated to capture 3D effects.

First, the burners considered in Fig. 9 are long narrow tubes for which end effects modify acoustic modes. In the low-frequency range, this can be accounted for [40] and a standard length

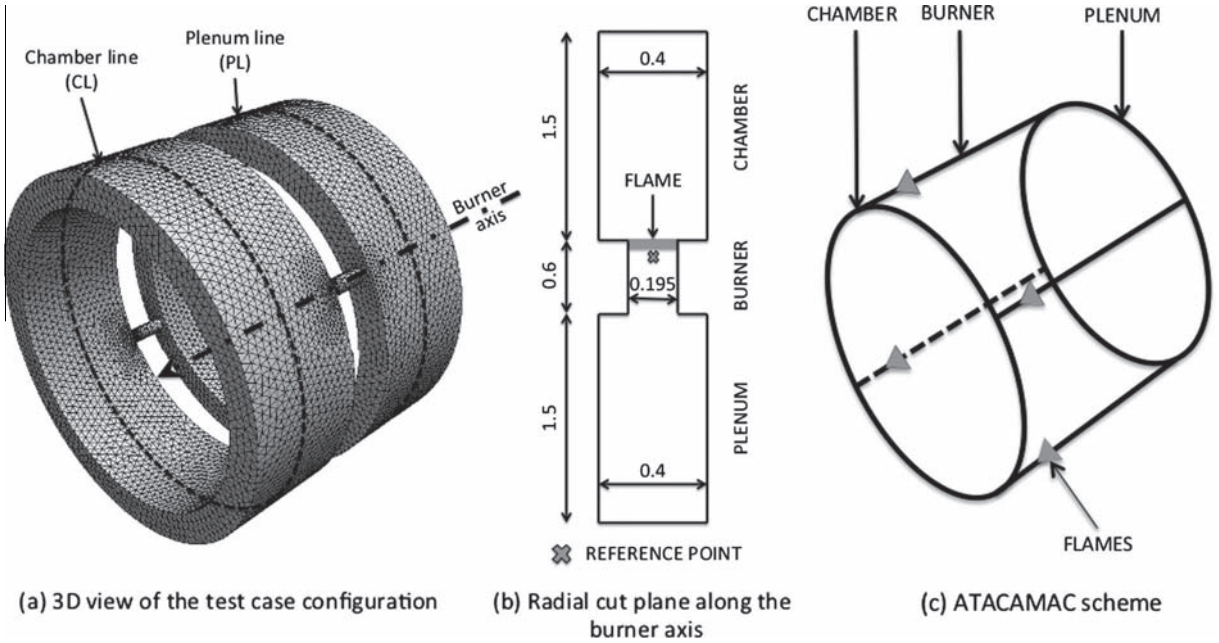

Fig. 9. 3D toy model to validate the ATACAMAC methodology. Perfect annular chamber and plenum connected by four burners ($N = 4$). – – –: Line in the plenum (PL) and in the chamber (CL) along which absolute pressure and phase will be plotted.

correction for a flanged tube [41] is applied at the two burner's ends. The corrected length L_i for the burners is

$$L_i = L_i^0 + 2 \times 0.4\sqrt{4S_i/\pi}, \tag{42}$$

where L_i^0 is the ith burner length without correction and S_i is the surface of the ith burner.

Second, the position of the compact flames is defined via the parameter $\alpha = z_{f,i}/L_i$, where L_i is the corrected burner length and $z_{f,i}$ is the position of the center of the flame. In Sections 5 and 6, the flame position parameter is set to $\alpha = 0.88$, a location chosen because it is far away from all pressure nodes.

5. Mode analysis of a weakly coupled PBC configuration with four burners ($N = 4$)

Under the weak-coupling-factors assumption ($0 < \wp_{p,i} \ll 1$ and $0 < \wp_{c,i} \ll 1$), frequencies of the whole system can be analyzed assuming small perturbations around the chamber alone (FDCp mode at $k^0 L_c = p\pi$) or plenum alone (FDPp mode at $k_u^0 L_p = p\pi$), wavenumbers leading to two families of modes that appear separately (Section 3.3),

$$kL_c = p\pi + \epsilon_c \text{ (WCCp modes)} \tag{43}$$

or

$$k_u L_p = p\pi + \epsilon_p \text{ (WCPp modes)}, \tag{44}$$

where p is the mode order, $\epsilon_c \ll p\pi$, and $\epsilon_p \ll p\pi$. Since the two families of modes behave in the same manner (only radius, density, and sound speed are changed), only weakly coupled chamber modes will be detailed in this section.

Due to symmetry considerations of the case $N = 4$, odd-order modes ($p = 2q + 1, q \in \mathbb{N}$), and even-order modes ($p = 2q, q \in \mathbb{N}$) will not behave in the same manner and are analyzed in Sections 5.1 and 5.2, respectively.

5.1. Odd-order weakly coupled modes of the PBC configuration with four burners ($N = 4$)

Considering odd-order modes ($p = 2q + 1, q \in \mathbb{N}$) with the low-coupling-limit assumption ($0 < \wp_{p,i} \ll 1$ and $0 < \wp_{c,i} \ll 1$) leads to the expansion $kL_c = p\pi + \epsilon_c$ (for a WCCp mode). A Taylor expansion can therefore be used to obtained a simplified analytical expression for the transfer matrix of the ith sector and consequently for the dispersion relation (Eq. (25)). This approach is fully detailed in Appendix A for the first mode on a single-burner case ($N = 1$) for simplicity. The same approach for the pth mode and four burners ($N = 4$) leads (see Table A.1) to

$$\sin(p\pi\beta)^2\left[\epsilon_c^2 + 4\epsilon_c\Gamma_4^0 + 4\Gamma_4^{0^2}\right] + o(\epsilon_c^2) = 0, \tag{45}$$

where $\beta = \frac{c^0 L_p}{c_u^0 L_c}$ and Γ_4^0 is the value of Γ_4 when $kL_c = p\pi$. Note that all the burners share the same length and cross section in this configuration, so the index i of Eq. (20) was removed for simplicity.

The β parameter can be viewed as a tuning parameter between cavities: it compares the period of the azimuthal modes in the plenum alone $\left(\tau_p^0 = \frac{2L_p}{pc_u^0}\right)$ and in the chamber alone $\left(\tau_c^0 = \frac{2L_c}{pc^0}\right)$. In general, the two annular volumes are not tuned and the periods τ_p^0 and τ_c^0 of the azimuthal modes of the plenum and the chamber do not match; i.e., $\beta = \tau_p^0/\tau_c^0 \neq l,\ l \in \mathbb{N}$ (for example, for the first chamber and plenum modes ($p = 1$) of Table 1 where $\beta \simeq 1.60$), so that the only solution to satisfy Eq. (45) is

$$\epsilon_c^2 + 4\epsilon_c\Gamma_4^0 + 4\Gamma_4^{0^2} + o(\epsilon_c^2) = 0. \tag{46}$$

This quadratic equation has a double root,[3]

[3] This approach can be extended at higher orders to unveil plenum/chamber interactions. From a third-order truncation of the dispersion relation (Eq. (25)), a second-order correction on eigenfrequencies found in Eq. (47) is obtained for WCCp modes,

$$\epsilon_c = -2\Gamma_4^0 - H(\beta)\Gamma_2^0\Gamma_3^0 \text{ (WCCp modes)},$$

where $H(\beta) = 4\tan(p\pi\beta/2)$.

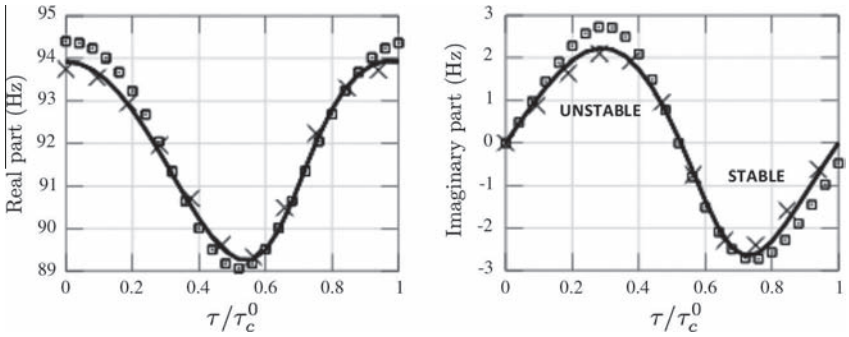

Fig. 10. Eigenfrequency of the WCC1 mode for four burners ($N = 4$) with $n_i = 1.57$ as a function of τ/τ_c^0. ——: Numerical resolution of the dispersion relation Eq. (25). □: Analytical model prediction Eq. (47). ×: AVSP results.

$$\epsilon_c = -2\Gamma_4^0, \tag{47}$$

where Γ_4^0 is the value of Γ_4 (Eq. (20)) at $\omega = \omega^0 = p\pi c^0/L_c$.

Real and imaginary parts of the frequency obtained in Eq. (47) are compared with the exact numerical resolution of the dispersion relation Eq. (25) and with AVSP results in Fig. 10. Very good agreement, is found showing that the asymptotic expression for the frequency (Eq. (47)) is correct.

From Eq. (47), a simple analytical stability criterion can be derived as explained in Appendix B for weakly coupled chamber modes (Eq. (B.3)),

$$\underbrace{\sin\left(2\pi\frac{\tau}{\tau_c^0}\right)}_{\text{effect of } \tau}\ \underbrace{\sin\left(2p\pi\frac{\alpha L_i c^0}{L_c c_u^0}\right)}_{\text{effect of } \alpha} < 0 \quad \text{(WCCp modes)}, \tag{48}$$

where $\tau_c^0 = \frac{2c^0}{pL_c}$.

Time delay τ of the FTF and flame position α have an effect on the stability and can be studied separately:

- **Time delay**—From Eq. (48), a critical time delay controlling the transition from stable to unstable regimes can be obtained: $\tau_{\text{crit}} = \tau_c^0/2 = \frac{L_c}{pc^0}$ for WCCp modes. This result being also valid for plenum modes (i.e., WCPp modes; see Eq. (B.4) leading to the critical time delay $\tau_p^0/2 = \frac{L_p}{pc_u^0}$), stability ranges of the two first azimuthal modes WCC1 and WCP1 can be displayed simultaneously (Fig. 11). This shows that the region where both the chamber and plenum modes are stable is smaller than the stability ranges of modes taken separately: stabilizing one mode of the system cannot ensure the stability of the whole system. Of course, this result does not include any dissipation or acoustic fluxes through the boundaries [42], which would increase stability regions.
- **Flame position**—Similarly to longitudinal modes in the Rijke tube [2,26,43], the flame position (defined by α) also controls the stability (Eq. (48)). Appendix C demonstrates an analytical expression for the critical flame position for weakly coupled modes (Eq. (C.2)) at which the stability change occurs. These expressions are close to the solution found in Rijke tubes (Eq. (C.1)) and have been validated for several weakly coupled modes (Table C.1 and Fig. C.1).

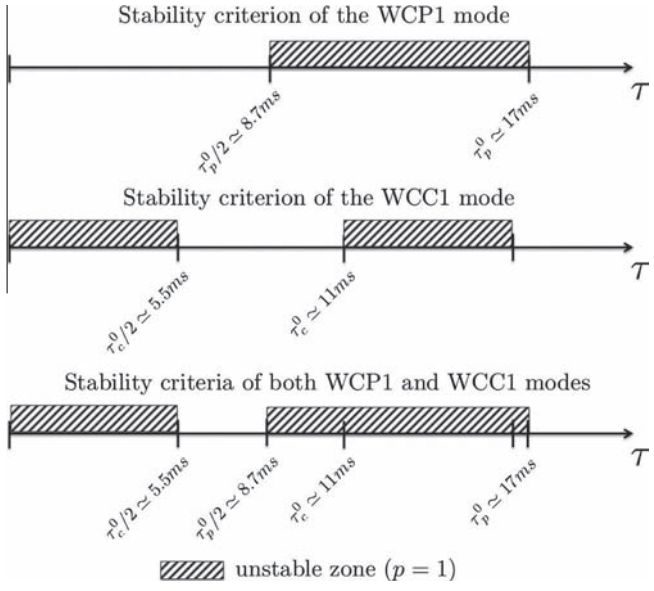

Fig. 11. Stability maps (Eq. (48)) of the two first azimuthal modes ($p = 1$) for a flame located at $\alpha \simeq 0.88$: WCP1 (top), WCC1 (middle), and both WCP1 and WCC1 (bottom).

5.2. Even-order modes of the PBC configuration with four burners ($N = 4$)

Assuming even-order weakly coupled chamber modes ($p = 2q, q \in \mathbb{N}$) and using Eq. (25) with the low-coupling-limit assumption ($0 < \wp_{p,i} \ll 1$ and $0 < \wp_{c,i} \ll 1$), the dispersion relation (Eq. (25)) becomes (Table A.1)

$$\sin(p\pi\beta/2)^2\left[\epsilon_c^2 + 4\epsilon_c\Gamma_4^0\right] + o(\epsilon_c^2) = 0, \tag{49}$$

where $\beta = \frac{k_u L_p}{kL_c}$ and Γ_4^0 is the value of Γ_4 when $kL_c = p\pi$.

When chamber and plenum frequencies do not match, i.e., $\beta \neq 1$ (for example, for the second ($p = 2$) mode of Table 1, where $\beta \simeq 1.60$), the only solution to satisfying Eq. (49) is to have

$$\epsilon_c^2 + 4\epsilon_c\Gamma_4^0 + o(\epsilon_c^2) = 0. \tag{50}$$

This quadratic equation has two distinct roots:

$$\epsilon_c = 0 \quad \text{and} \quad \epsilon_c = -4\Gamma_4^0. \tag{51}$$

The first solution ($\epsilon_c = 0$) of Eq. (51) corresponds to modes that are not affected by the flames: the symmetry of the four-burners case ($N = 4$) allows even-order modes to impose a pressure node at each burner location, suppressing the flame effect on these modes, which become neutral.

The second solution of Eq. (51) $\left(\epsilon_c = -4\Gamma_4^0\right)$ correspond to modes that are strongly affected by the flame because it imposes a pressure anti-node (maximum pressure) downstream of each burner.

Real and imaginary parts of the frequency obtained from Eq. (51) are compared with the numerical solutions of the dispersion relation Eq. (25) and to AVSP results in Fig. 12. Very good

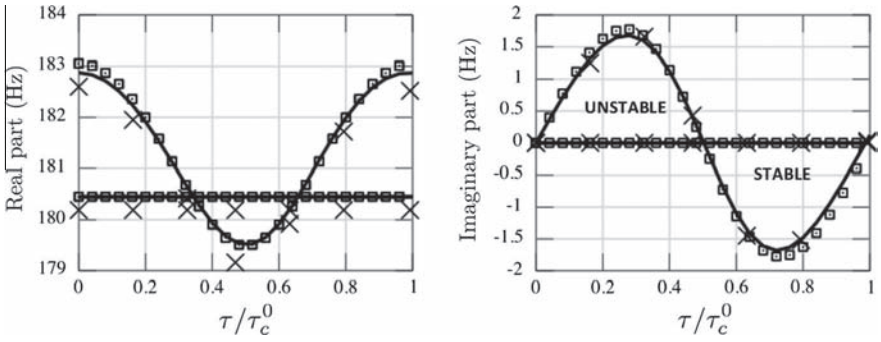

Fig. 12. Eigenfrequency of the WCC2 mode for four burners ($N = 4$) with $n_i = 1.57$ as a function of τ/τ_c^0. ——: Numerical resolution of the dispersion relation Eq. (25). □: Analytical model prediction Eq. (51). ×: AVSP results.

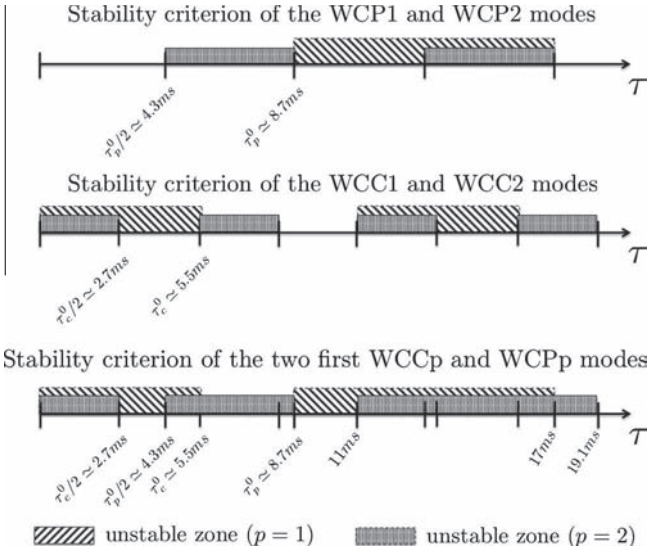

Fig. 13. Stability maps of the WCC1, WCC2, WCP1, and WCP2 modes.

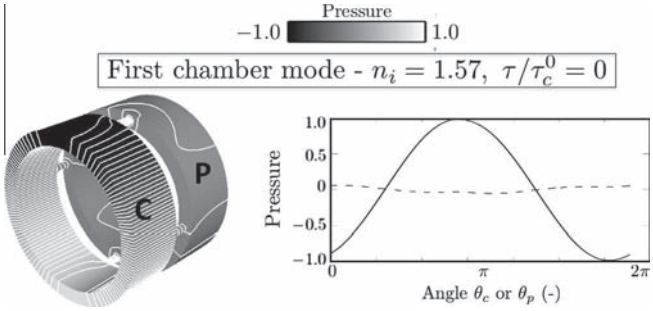

Fig. 14. Pressure mode structures ($p' = |p'|\cos(\arg(p'))$) obtained with AVSP with pressure isolines (left) and pressure along the azimuthal direction in the annular chamber (——) and annular plenum (– – –) for the WCC1 mode of a PBC configuration with four burners ($N = 4$) and $n_i = 1.57$ at the time delay $\tau/\tau_c^0 = 0$.

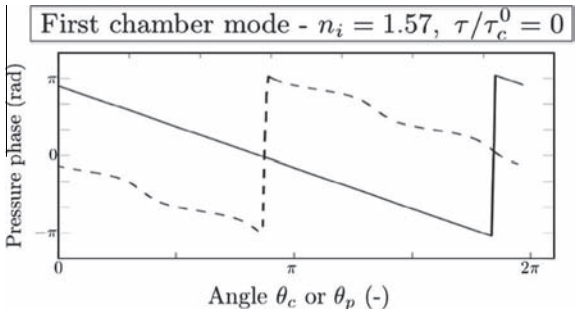

Fig. 15. Pressure phase of the WCC1 mode obtained with AVSP at $n_i = 1.57$ along the azimuthal direction in the annular chamber (——) and the annular plenum (– – –) for time delay $\tau/\tau_c^0 = 0$.

agreement is found and the nonperturbed mode ($\epsilon_c = 0$) is correctly captured (straight lines).

Using Eq. (51) and Appendix B leads to an analytical stability criterion for WCCp even-order modes (Eq. (B.3)). This result being also valid for WCPp modes (Eq. (B.4)) and using the results from Section 5.1, stability maps of the weakly coupled plenum and chamber modes (WCC1, WCC2, WCP1 and WCP2) can be plotted together (Fig. 13), highlighting the difficulty of getting a stable system in the absence of dissipation, as assumed here: considering only these four modes, no stable region is found for time delays lower than 19.1 ms in the case described in Table 1 (Fig. 13).

5.3. Mode structure of weakly coupled modes

In weakly coupled situations, acoustic activity is present only in one annular cavity and in the burners, as shown in Fig. 14 for the WCC1 mode (the same mode with the opposite rotation direction is also captured by AVSP but not shown here). Figure 15 shows that this mode is purely rotating in the chamber, while it is mixed in the plenum. Therefore, the combination of the two weakly coupled chamber modes with the clockwise rotation (shown in Fig. 15) and the counter clockwise rotation (not shown) make it possible to have purely rotating or purely standing modes, but not necessarily in the two annular cavities at the same time.

5.4. Stability map of weakly coupled situations

Sections 5.1 and 5.2 focused on weakly coupled situations where the low-coupling-factor assumption ($\wp_p \ll 1$ and $\wp_c \ll 1$) is valid. Stability maps of perturbed modes (i.e., $\epsilon \neq 0$) in the complex plane $[Re(f), Im(f)]$ are well suited to show differences between the several regimes—weakly coupled and strongly coupled situations. These maps are oriented circles (– – –) (WCP1) and —— (WCC1) in Fig. 16) centered at the frequency $f(n_i = 0) \simeq f_0$, which corresponds to a passive flame mode ($n_i = 0$: × in Fig. 16) and is approximately the frequency of the cavity alone $\left(f_0 = \frac{pc^0}{2L}\right)$. The radius is proportional to the coupling factor, which can be increased via the surface ratios (S_i/S_p and S_i/S_c) or the flame interaction index n_i. In the weakly coupled regime, WCCp and WCPp modes do not strongly interact, as shown in Fig. 16: modes in the plenum and in the chamber live separately.

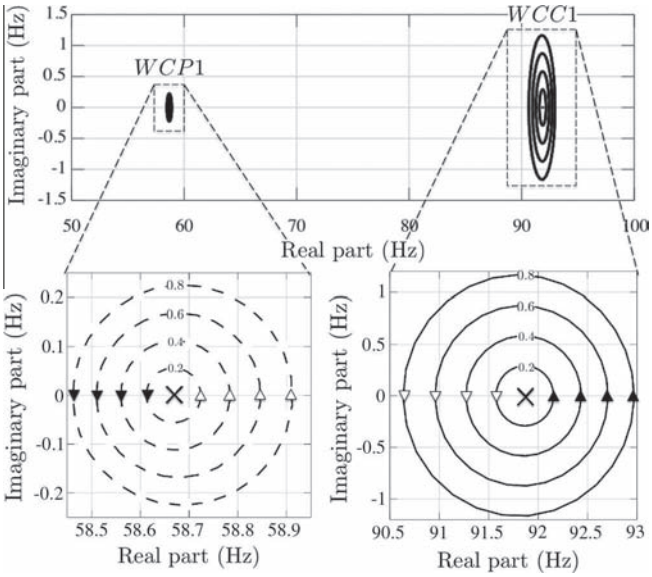

Fig. 16. Eigenfrequencies of both WCP1 and WCC1 modes (top) and zoom on WCP1 (bottom left) and WCC1 (bottom right) when the flame delay changes for PBC configuration with four burners ($N = 4$) with $n_i = 0.2$, 0.4, 0.6, and 0.8. ×: Passive flame ($n_i = 0$). – – –: WCP1 mode. ——: WCC1 mode. ▶ : $\tau/\tau_p^0 = 0$ or $\tau/\tau_c^0 = 0$ oriented in the increasing τ direction, ▷ : $\tau/\tau_p^0 = 1/2$ or $\tau/\tau_c^0 = 1/2$.

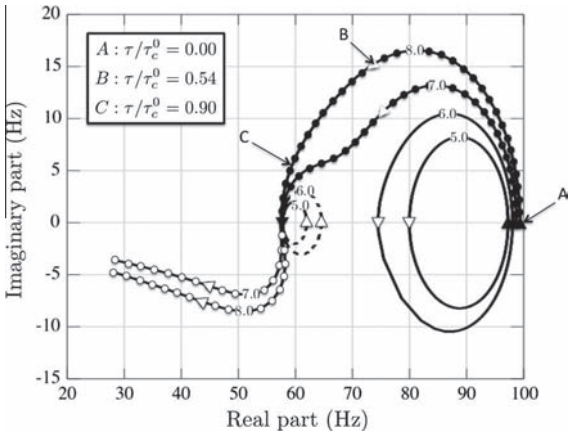

Fig. 17. Eigenfrequencies on the complex plane for a PBC configuration with four burners ($N = 4$). – – –: WCP1 mode ($n_i = 5.0$ and 6.0). ——: WCC1 mode ($n_i = 5.0$ and 6.0). ○: SC1 mode ($n_i = 7.0$ and 8.0). •: SC2 mode ($n_i = 7.0$ and 8.0). ▶ : $\tau/\tau_p^0 = 0$ or $\tau/\tau_c^0 = 0$ oriented in the increasing τ direction and ▷: $\tau/\tau_p^0 = 1/2$ or $\tau/\tau_c^0 = 1/2$.

6. Mode analysis of a strongly coupled PBC configuration with four burners ($N = 4$)

For weakly coupled cases (Section 5), the frequencies of the azimuthal modes in the plenum and in the chamber are only marginally affected by the flame (Figs. 10 and 12), so they can never match (Fig. 16). However, if the flame interaction index (n_i) is larger, the frequencies of the azimuthal modes of the annular plenum and the annular chamber change more and the possibility of having the two frequencies match opens an interesting situation where the whole system can resonate. This corresponds to the strongly coupled modes of order p (referred as "SCp" modes) studied in this section.

Figure 17 shows the stability maps of the WCC1 (——) and WCP1 (– – –) modes obtained with low flame-interaction index ($n_i = 5.0$ and 6.0), as well as the SC1 (○) and SC2 modes (•) obtained for higher flame-interaction index ($n_i = 7.0$ and 8.0[4] at the zero frequency limit). Three points in the SC2 trajectory with $n_i = 8.0$ corresponding to several time delays ($\tau/\tau_c^0 = 0$ (A), $\tau/\tau_c^0 = 0.54$ (B), and $\tau/\tau_c^0 = 0.9$ (C)) are displayed in Fig. 17 and will be used as typical cases to show pressure structures in the annular plenum and chamber.

For low flame interaction index ($n_i = 5.0$ and 6.0), the first two modes always have different frequencies and can be identified as plenum (WCPp: – – –) or chamber modes (WCCp: ——), as studied in Section 5.

However, for higher flame interaction indices ($n_i = 7.0$ and 8.0), a bifurcation occurs: frequencies of the annular plenum, burners, and annular chamber can match, leading to strongly coupled modes where the whole system resonates. The trajectory of the first strongly coupled mode (SC1: ○) goes from the WCP1 mode (for small time delays $\tau < \tau_p^0/2$) to a longitudinal mode (not presented here, around 40 Hz, for large time delays $\tau > \tau_p^0/2$). A second strongly coupled mode (SC2: •) has a trajectory in the complex plane coming from the WCC1 mode (for small time delays $\tau < \tau_c^0/2$) and going to the WCP1 mode (for large time delays $\tau > \tau_c^0/2$).

[4] Note that the typical order of magnitude of the interaction index n_i is $T_b/T_u - 1$.

The stability map of the SC2 mode (•) at $n_i = 8.0$ has been validated against the 3D finite element solver AVSP (Fig. 18). Good agreement between AVSP (×) and the numerical resolution of Eq. (25) (——) is found. The growth rate is slightly underestimated, but the global trend is well captured: the mode is fully unstable for all time delays, which corresponds to a new behavior compared to the weakly coupled modes. The analytical approach developed in Section 5 for the weakly coupled regime (□ in Fig. 18) is not able to capture this new highly nonlinear behavior.

When the flame interaction index is sufficiently large ($n_i > 7.0$), i.e., when the flame is sufficiently intense, the modes of plenum and chamber lock in and become unstable for all time delays. Figure 19 shows the modulus of the coupling factors $\|\Gamma_1\|, \|\Gamma_4\|$ and the interaction product $\|\Gamma_2\Gamma_3\|$ (terms appearing in analytical results summarized in Table B.1) as a function of the time delay τ_1 for the three different cases corresponding to the first order ($p = 1$) chamber mode: $n_1 = 1.57$ (weakly coupled regime), $n_1 = 4.0$ (limit case between weakly/strongly coupled regimes), and $n_1 = 8.0$ (strongly coupled regime). It highlights the tuning mechanism:

- In the weakly coupled regime ($n_1 = 1.57$), both Γ_1 and Γ_4 have the same order of magnitude and they vary in opposite directions. The low-coupling-factors assumption is satisfied.
- Then, at the limit case between weakly and strongly coupled regimes ($n_1 = 4.0$), $\|\Gamma_4\|$ is almost constant with time delay τ_1. The other coupling factors are not affected.
- Finally, in the strongly coupled regime ($n_1 = 8.0$), the coupling parameter of the burner/chamber junction Γ_4 is amplified, which indicates that this junction is tuned. The evolution with the time delay is reversed compared to the weakly coupled regime: now, the two annular cavities (plenum and chamber) act together in the same manner; they are coupled. Consequently, the interaction term ($\|\Gamma_2\Gamma_3\|$) is also increased. The low-coupling-factors assumption is not satisfied in this case.

Pressure structures ($p' = |p'|\cos(\arg(p'))$) along the azimuthal direction in the plenum (PL line in Fig. 9) and in the chamber (CL line in Fig. 9) obtained with AVSP for the second strongly coupled mode are displayed in Fig. 20 for a high flame-interaction index ($n_i = 8.0$) and several time delays (A: $\tau/\tau_c^0 = 0$, B: $\tau/\tau_c^0 = 0.54$, and C: $\tau/\tau_c^0 = 0.9$ from Fig. 17). For null time delays (A in Fig. 17), acoustic activity is only present in the chamber (——) and the frequency is close to the weakly coupled chamber mode. The acoustic activity in the second annular cavity (i.e., the plenum:

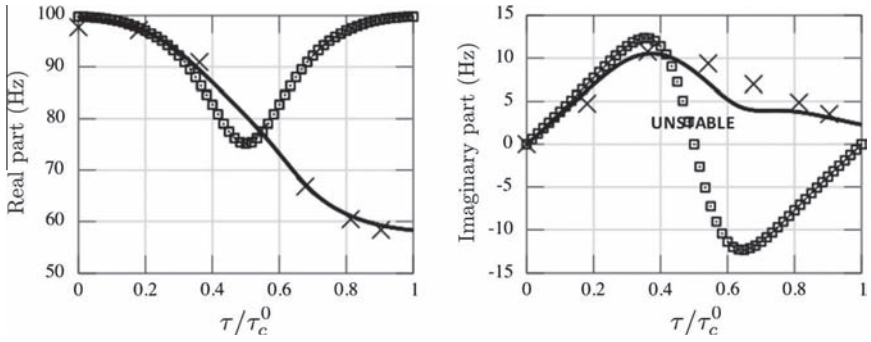

Fig. 18. Eigenfrequency of the first-order chamber mode ($p = 1$) for four burners ($N = 4$) as a function of τ/τ_c^0 with $n_i = 8.0$. ——: Numerical resolution of Eq. (25). □: Analytical model prediction for weakly coupled situations (Eq. (47)). ×: AVSP results.

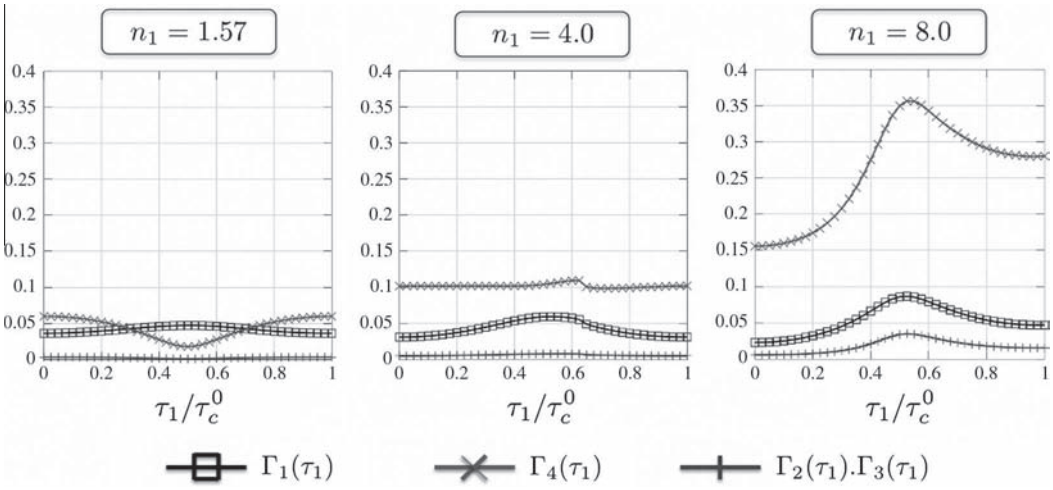

Fig. 19. Modulus of the coupling factors $\|\Gamma_1\|$ (□), $\|\Gamma_4\|$ (×), and $\|\Gamma_2 * \Gamma_3\|$ (+) varying with the time delay τ_1 for three cases: $n_1 = 1.57$ (weakly coupled regime), $n_1 = 4.0$ (limit case), and $n_1 = 8.0$ (strongly coupled regime).

– – –) grows with the time delay τ. For $\tau/\tau_c^0 = 0.54$ ms (B in Fig. 17), a strong interaction with the burners appears leading to higher growth rates. Surprisingly, this case corresponds only to moderate acoustic activity in the second annular cavity (i.e., the annular plenum: – – –). For $\tau/\tau_c^0 = 0.9$ (C in Fig. 17), a first-order mode is present in both annular cavities highlighting a strongly coupled situation. This strong interaction between plenum and chamber revealed by the presence of acoustic activity in both annular cavities leads, however, to a marginally unstable mode.

Figure 21 shows the pressure phase in the annular plenum (– – –) and in the annular chamber (——) for several time delays. The same mode with opposite direction is also found with AVSP but not shown here. For small time delay ($\tau/\tau_c^0 = 0$ for case A and $\tau/\tau_c^0 = 0.54$ for case B of Fig. 17), pressures in the plenum and in the chamber have different natures: purely spinning mode in the chamber (linear phase) and a mixed mode in the plenum (wave shape of the phase). The combination of clockwise and counter clockwise mode can generate purely spinning or purely standing mode but not necessarily in both annular cavities at the same time. However, higher time delay cases (such as case C, where $\tau/\tau_c^0 = 0.9$) correspond to strongly coupled situations where both annular cavities lock in (Fig. 20C). In this case, pressure in the chamber and plenum exhibit the same nature: purely spinning in both cavities in Fig. 21C (the same mode with the opposite rotating direction is also found by AVSP but not shown here). The combination of the purely spinning modes (clockwise and counter clockise) can also lead to standing modes in both annular cavities at the same time. This is a specific behavior only encountered in locked-in modes as case C.

Finally, it is demonstrated that a highly unstable mode does not necessarily exhibit strong acoustic activity in both annular cavities (as for case B) and that a mode where acoustic activity appears in the whole system can be only marginally unstable (as for case C). Moreover, the phase lag between pressure in the annular cavity and in the annular chamber as well as the nature of the mode (spinning, standing, or mixed), changes when acoustic activity is present in both annular cavities, a property that could be checked experimentally.

7. Conclusion

To complement expensive large eddy simulation [44] and Helmholtz [38] 3D codes used to study azimuthal modes in annular combustors, simple tools are required to understand the physics of these modes and create predesigns of industrial combustors. This paper describes a simple analytical theory to compute the azimuthal modes appearing in these combustors. It is based on a quasi-one-dimensional acoustic network where N burners are connected to an annular plenum and chamber. A manipulation of the corresponding acoustic equations in this configuration leads to a simple analytical dispersion relation that can be solved numerically. This method makes it possible to exhibit coupling factors between plenum, burners, and chamber that depend on area ratios and flame transfer function (FTF). For $N = 4$, a fully analytical resolution can be performed in specific situations where coupling factors of the FTF [22,26] are small and simple stability criteria can be

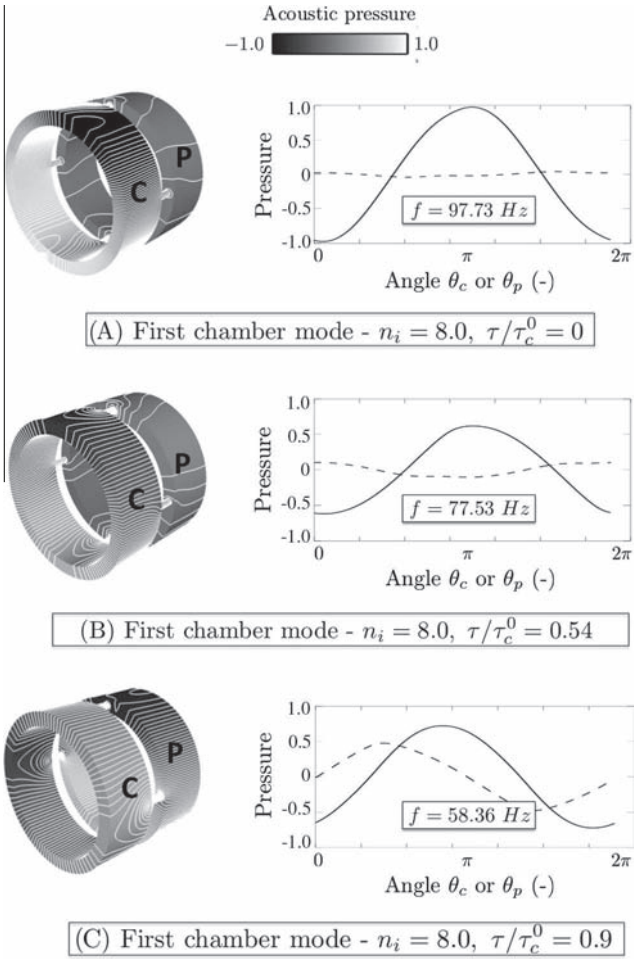

Fig. 20. Pressure structures and isolines ($p' = |p'|\cos(\arg(p'))$) obtained with AVSP (left) and pressure along the azimuthal direction in the annular chamber (——) and annular plenum (– – –) for the SC2 mode of a PBC configuration with four burners ($N = 4$) and $n_i = 8.0$ at several time delays: $\tau/\tau_c^0 = 0$ (top), 0.54 (middle), and 0.9 (bottom). The configuration corresponds to $f_{FDP1} = 56$ Hz and $f_{FDC1} = 90$ Hz.

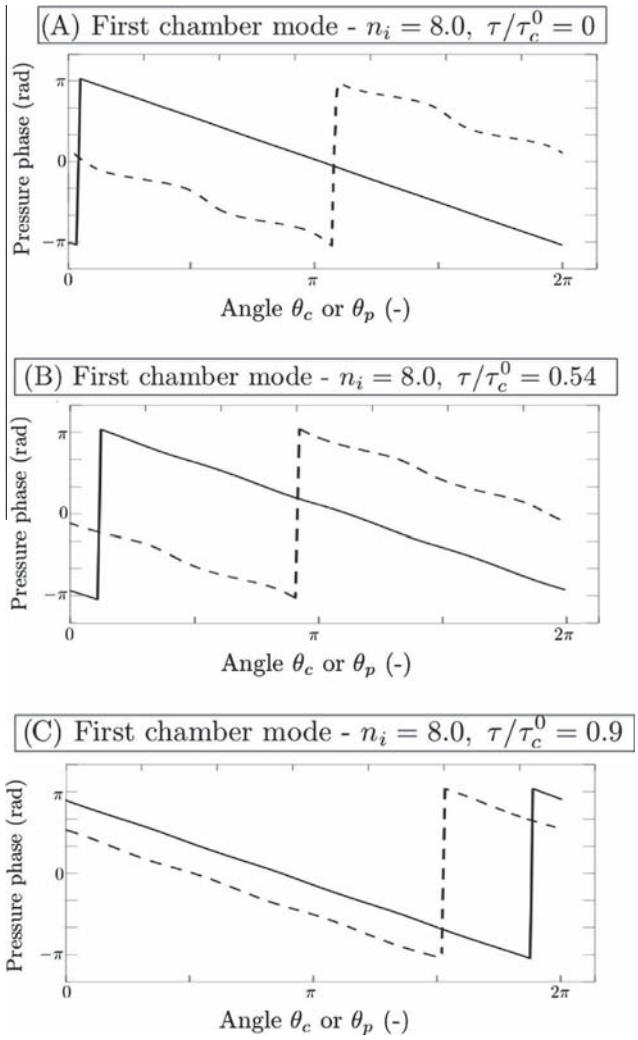

Fig. 21. Pressure phase obtained with AVSP for the SC2 mode at $n_i = 8.0$ along the azimuthal direction in the annular chamber (——) and the annular plenum (– – –) for several time delays: $\tau/\tau_c^0 = 0$ (top), 0.54 (middle), and 0.9 (bottom).

proposed. For higher coupling factors, a bifurcation occurs, yielding a strongly coupled regime where acoustic activity is present in both annular cavities. The nature of such a mode (standing, spinning, or mixed) changes with the time delay. Purely spinning or purely standing modes in the annular plenum and in the chamber were found simultaneously only when a strongly coupled situation occurred (Fig. 21 C). For strongly coupled cases, a PBC configuration where two annular cavities are connected to N burners is required to predict correctly eigenmodes and stability maps. This analytical tool has been compared systematically to the predictions of a full three-dimensional Helmholtz solver. A very good agreement is found, showing that the present asymptotic resolution is correct.

These results show that a simple analytical formulation for studying azimuthal modes in annular combustors is an interesting tool that can be used as a predesign tool or as a help to postprocess acoustic or LES simulations.

Appendix A. Analytical dispersion relation of a PBC configuration with a single burner ($N = 1$)

The analytical dispersion relation (Eq. (25)) is obtained for a general PBC configuration with N burners. To explain the ATACAMAC approach leading to the analytical eigenfrequencies of the system, the case of a single burner ($N = 1$) will be detailed.[5]

Considering only one burner, the transfer matrix $M = R_1 T_1 - Id$ of the whole system is

$$M = \begin{bmatrix} \cos(2k_u L_p) - 1 & -\sin(2k_u L_p) & \cdots & 0 & 0 \\ \sin(2k_u L_p) + 2\cos(2k_u L_p)\Gamma_1 & -2\sin(2k_u L_p)\Gamma_1 + \cos(2k_u L_p) - 1 & & 2\cos(2kL_c)\Gamma_2 & -2\sin(2kL_c)\Gamma_2 \\ 0 & 0 & & \cos(2kL_c) - 1 & -\sin(2kL_c) \\ 2\cos(k_u L_p)\Gamma_3 & -2\sin(2k_u L_p)\Gamma_3 & & \sin(2kL_c) + 2\cos(2kL_c)\Gamma_4 & -2\sin(2kL_c)\Gamma_4 + \cos(2kL_c) - 1 \end{bmatrix}. \tag{A.1}$$

[5] Since there is only one burner, the index i has been omitted to simplify notation (e.g., Γ_1 instead of $\Gamma_{i=1,1}$).

Table A.1
Analytical expressions of wavenumber perturbation for WCCp and WCPp azimuthal modes.

Type	Odd/even	Second-order dispersion relation ($o(\epsilon^2)$)
WCC	Odd	$\sin(p\pi\beta)\left[\epsilon^2+4\epsilon\Gamma_4^0+4\Gamma_4^{0^2}\right]=0$
	Even	$\sin(p\pi\beta/2)\left[\epsilon^2+4\epsilon\Gamma_4^0\right]=0$
WCP	Odd	$\sin(p\pi/\beta)\left[\epsilon^2+4\epsilon\Gamma_1^0+4\Gamma_1^{0^2}\right]=0$
	Even	$\sin(p\pi/(2\beta))\left[\epsilon^2+4\epsilon\Gamma_1^0\right]=0$

In the general case with N burners, a Taylor expansion of this matrix has to be performed as a first simplification. Here, the matrix is simple enough to compute analytically the determinant leading to the exact dispersion relation

$$\begin{aligned}&(\Gamma_1\Gamma_4-\Gamma_2\Gamma_3)\sin(2kL_c)\sin(2k_uL_p)+2\Gamma_1[1-\cos(2kL_c)]\sin(2k_uL_p)\\&+2\Gamma_4[1-\cos(2k_uL_p)]\sin(2kL_c)\\&+4[1-\cos(2kL_c)][1-\cos(2k_uL_p)]=0.\end{aligned}\tag{A.2}$$

The dispersion relation, Eq. (A.2), is nonlinear. The idea is to use a Taylor expansion at the second (or third) order and to solve it analytically. The expansion has to be done around a FDCp (i.e., $kL_c=p\pi+\epsilon_c$) or FDPp (i.e., $k_uL_p=p\pi+\epsilon_p$) mode (see Section 3.3 for details). For instance, in the case of the WCC1 mode ($kL_c=\pi+\epsilon$, which implies $k_uL_p=\beta(\pi+\epsilon_c)$, where $\beta=\frac{c^0L_p}{c_u^0L_c}$), the dispersion relation Eq. (A.2) becomes

$$[\cos(2\pi\beta)-1]\left[\epsilon_c\Gamma_4^0+\epsilon_c^2+o\left(\epsilon_c^2\right)\right]=0,\tag{A.3}$$

where Γ_4^0 is the value of Γ_4 evaluated at $kL_c=p\pi$.

Note that solutions of Eq. (A.3) being $\epsilon_c=-\Gamma_4^0$, the term $\epsilon_c\Gamma_4^0$ is of the same order of magnitude as ϵ_c^2 and therefore has to be kept in the analytical dispersion relation, Eq. (A.2).

Analytical dispersion relations for $N>1$ are more complex to derive but follow a similar procedure. When $N=4$, the dispersion relations of Table A.1 are obtained.

Appendix B. Stability criterion of weakly coupled modes for a four-burner configuration ($N=4$)

A mode is stable if the imaginary part of the wavenumber is negative. Table B.1 shows analytical expressions for the wavenumber perturbation ϵ for WCPp and WCCp modes.[6]

Analytical stability criteria can be derived by calculating the sign of $\mathrm{Im}\left(\Gamma_1^0\right)$, $\mathrm{Im}\left(\Gamma_4^0\right)$, and $\mathrm{Im}\left(\Gamma_2^0\Gamma_3^0\right)$ using the following definitions: $\mathbb{F}^*$ is the complex conjugate of the flame parameter $\mathbb{F}=\frac{\rho^0c^0}{\rho_u^0c_u^0}\left(1+n.e^{i\omega^0\tau}\right)$, $\theta^0=\omega^0(1-\alpha)L_i/c^0\in\mathbb{R}$, and $\theta_u^0=\omega^0\alpha L_i/c_u^0\in\mathbb{R}$. The notation $\mathfrak{D}$ refers to $\mathfrak{D}=|\cos(\theta^0)\sin(\theta_u^0)+\mathbb{F}\sin(\theta^0)\cos\left(\theta_u^0\right)|^2$.

With these notations, the signs of the imaginary parts of these coupling parameters are

$$\mathrm{Im}\left(\Gamma_1^0\right)=\frac{S_i}{4S_p\mathfrak{D}}\sin(2\theta^0)\mathrm{Im}(\mathbb{F})\tag{B.1}$$

$$\mathrm{Im}\left(\Gamma_4^0\right)=-\frac{S_i}{4S_c\mathfrak{D}}\sin\left(2\theta_u^0\right)\mathrm{Im}(\mathbb{F}).\tag{B.2}$$

Eqs. (B.1) and (B.2) lead to simple analytical stability criteria for WCCp and WCPp modes:

[6] Since all sectors are identical, the index i has been omitted to simplify notations (e.g. Γ_1 instead of $\Gamma_{i,1}$).

Table B.1
Analytical expressions for wavenumber perturbation ϵ for WCCp and WCPp modes where $H(x)=4\tan(p\pi x/2)$ and $G(x)=4\frac{\sin(p\pi x/2)}{\cos(p\pi x/2)-(-1)^{p/2}}$ have real values.

Type	Odd/even	Wavenumber perturbation (ϵ)
WCC	Odd	$-2\Gamma_4^0-H(\beta)\Gamma_2^0\Gamma_3^0$
	Even	$-2\Gamma_4^0-G(\beta)\Gamma_2^0\Gamma_3^0$
WCP	Odd	$-2\Gamma_1^0-H(1/\beta)\Gamma_2^0\Gamma_3^0$
	Even	$-2\Gamma_1^0-G(1/\beta)\Gamma_2^0\Gamma_3^0$

$$\sin\left(2\pi\tau/\tau_c^0\right)\sin\left(2p\pi\frac{\alpha L_ic^0}{L_cc_u^0}\right)<0\quad\text{for WCCp modes}\tag{B.3}$$

$$\sin\left(2\pi\tau/\tau_p^0\right)\sin\left(2p\pi\frac{(1-\alpha)L_ic_u^0}{L_pc^0}\right)>0\quad\text{for WCPp modes.}\tag{B.4}$$

Appendix C. Flame position effect on annular combustor stability

Similarly to longitudinal modes in the Rijke tube [2,26,43], the flame position (defined by α) also controls the stability (Eq. (48)). In a quasi-isothermal Rijke tube, for common (small) values of the FTF time delay τ, stability of the first longitudinal mode is obtained only when the flame is located in the upper half of the tubes [45,46], i.e., $\alpha>1/2$, which can be extended for the pth longitudinal mode:

$$\frac{2m+1}{2p}<\alpha<\frac{2(m+1)}{2p},\quad\forall m\in\mathbb{N}\quad\text{(Rijke tube)}.\tag{C.1}$$

Eq. (48) highlights a similar behavior for azimuthal modes in a PBC configuration: for a WCCp mode with small values of the time delay $\tau<\tau_c^0/2$, $\sin\left(2\pi\frac{\tau}{\tau_c^0}\right)$ is positive and Eq. (48) leads to

$$\frac{2m+1}{2p}\frac{L_cc_u^0}{L_ic^0}<\alpha<\frac{2(m+1)}{2p}\frac{L_cc_u^0}{L_ic^0},\quad\forall m\in\mathbb{N}\quad\text{(WCCp modes)}.\tag{C.2}$$

Usually, the critical flame position $\alpha_{\mathrm{crit}}=\frac{L_cc_u^0}{2pL_ic^0}$ is larger than unity because the half-perimeter of the annular cavity is much longer than the burner length ($L_c\gg L_i$). Since the range of the normalized flame position α is [0–1], the flame position may affect the stability only for high-order modes (i.e., p large enough to get $\alpha_{\mathrm{crit}}<1$). For instance, in the case described in Table 1 with the corrected burner length $L_i\simeq0.76$ m, the critical flame positions α_{crit} and the stability ranges (Eq. (C.2)) are shown in Table C.1.

The change of stability with the flame position α for small time delays predicted in Table C.1 has been validated using the numerical resolution of the dispersion relation (Eq. (25)) in Fig. C.1. The critical flame positions obtained in Table C.1 are well captured for all modes. A situation where the plenum/chamber interaction is not negligible is shown for the WCC1 mode with $\alpha=0.3$ (i.e., the flame is close to the pressure node imposed by the large annular plenum).

Table C.1
Critical flame positions α_{crit} and flame positions satisfying Eq. (C.2) for WCCp odd-order modes of the case described in Table 1.

Mode order (p)	$p=1$	$p=3$	$p=5$	$p=7$
$\alpha_{\mathrm{crit}}=\frac{L_cc_u^0}{2pL_ic^0}$	2.70	0.9	0.54	0.39
α Satisfying Eq. (C.2)	none	[0.9–1]	[0.54–1]	[0.39–0.78]

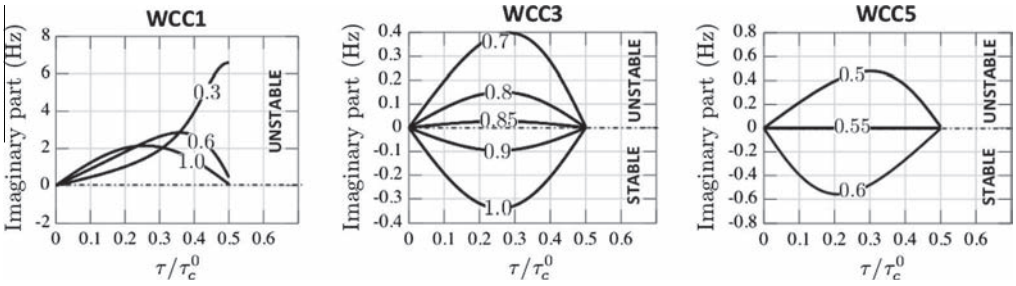

Fig. C.1. Growth rate for several flame positions α of the WCC1 ($\alpha = 0.3, 0.6, 1.0$—left), WCC3 ($\alpha = 0.5, 0.8, 0.85, 0.9, 1.0$—middle), and WCC5 ($\alpha = 0.5, 0.55, 0.6$—right) modes for small time delays ($\tau/\tau_c^0 < 1/2$) using the numerical resolution of the dispersion relation (Eq. (25)) with $n_i = 1.57$.

References

[1] W. Krebs, P. Flohr, B. Prade, S. Hoffmann, Combust. Sci. Technol. 174 (2002) 99–128.
[2] T. Poinsot, D. Veynante, Theoretical and Numerical Combustion, 3rd ed., 2011 <http://www.cerfacs.fr/elearning>.
[3] T. Lieuwen, V. Yang, in: Combustion Instabilities in Gas Turbine Engines. Operational Experience, Fundamental Mechanisms and Modeling, Progress in Astronautics and Aeronautics, vol. 210, AIAA, 2005.
[4] N. Worth, J. Dawson, Proc. Combust. Inst. 34 (2013) 3127–3134.
[5] N. Noiray, M. Bothien, B. Schuermans, Combust. Theory Model. (2011) 585–606.
[6] J. Kopitz, A. Huber, T. Sattelmayer, W. Polifke, in: Int'l Gas Turbine and Aeroengine Congress & Exposition, ASME GT2005-68797, Reno, NV, USA.
[7] S.R. Stow, A.P. Dowling, in: ASME Paper 2003-GT-38168, Atlanta, Georgia, USA.
[8] S. Evesque, W. Polifke, in: International Gas Turbine and Aeroengine Congress & Exposition, ASME Paper, vol. GT-2002-30064.
[9] S.R. Stow, A.P. Dowling, in: ASME Paper, 2001-GT-0037, New Orleans, Louisiana.
[10] D. Fanaca, P. Alemela, F. Ettner, C. Hirsch, T. Sattelmayer, B. Schuermans, in: ASME Turbo Expo, GT2008-50781.
[11] D. Fanaca, P. Alemela, C. Hirsch, T. Sattelmayer, B. Schuermans, J. Eng. Gas Turbines Power 132 (2010) 071502.
[12] J.-F. Bourgouin, D. Durox, T. Schuller, J. Beaunier, S. Candel, Combust. Flame 160 (2013) 1398–1414.
[13] K. Kunze, C. Hirsch, T. Sattelmayer, in: ASME Turbo Expo, GT2004-53106.
[14] J. Moeck, M. Paul, C. Paschereit, in: ASME Turbo Expo 2010 GT2010-23577.
[15] J.-F. Bourgouin, D. Durox, J. Moeck, T. Schuller, S. Candel, in: ASME Turbo Expo, GT2013-95010.
[16] C. Fureby, Flow Turb. Combust. 84 (2010) 543–564.
[17] P. Wolf, G. Staffelbach, L. Gicquel, J. Muller, T. Poinsot, Combust. Flame 159 (2012) 3398–3413.
[18] M. Leyko, F. Nicoud, S. Moreau, T. Poinsot, C. R. Acad. Sci. Méc. 337 (2009) 415–425.
[19] C. Sensiau, F. Nicoud, T. Poinsot, Int. J. Aeroacoust. 8 (2009) 57–68.
[20] G. Campa, S. Camporeale, A. Guaus, J. Favier, M. Bargiacchi, A. Bottaro, E. Cosatto, G. Mori, GT2011-45969.
[21] C. Pankiewitz, T. Sattelmayer, ASME J. Eng. Gas Turbines Power 125 (2003) 677–685.
[22] J. Parmentier, P. Salas, P. Wolf, G. Staffelbach, F. Nicoud, T. Poinsot, Combust. Flame 159 (2012) 2374–2387.
[23] G. Ghirardo, M. Juniper, Proc. Roy. Soc. A 469 (2013).
[24] S. Evesque, W. Polifke, C. Pankiewitz, in: 9th AIAA/CEAS Aeroacoustics Conference, vol. AIAA paper 2003-3182.
[25] B. Schuermans, C. Paschereit, P. Monkewitz, in: 44th AIAA Aerospace Sciences Meeeting and Exhibit, 2006-0549.
[26] T. Schuller, D. Durox, P. Palies, S. Candel, Combust. Flame 159 (2012) 1921–1931.
[27] S. Stow, A. Dowling, in: ASME Turbo Expo, GT2004-54245.
[28] P. Palies, D. Durox, T. Schuller, S. Candel, Combust. Flame 158 (2011) 1980–1991.
[29] P. Huerre, P. Monkewitz, Annu. Rev. Fluid Mech. 22 (1990) 473–537.
[30] F.E. Marble, S. Candel, J. Sound Vibrat. 55 (1977) 225–243.
[31] G. Staffelbach, L. Gicquel, G. Boudier, T. Poinsot, Proc. Combust. Inst. 32 (2009) 2909–2916.
[32] J. O'Connor, T.Lieuwen, Phys. Fluids 24 - 075107 (2012a).
[33] J. O'Connor, T.Lieuwen, J. Eng. Gas Turbines Power 134 - 011501 (2012b).
[34] N. Worth, J. Dawson, Combust. Flame 160 (2013) 2476–2489.
[35] U. Krueger, J. Hueren, S. Hoffmann, W. Krebs, P. Flohr, D. Bohn, in: ASME Turbo Expo, 2000-GT-0095, Munich, Germany.
[36] W. Krebs, G. Walz, P. Flohr, S. Hoffmann, in: ASME Turbo Expo, 2001-GT-42.
[37] L. Crocco, J. Am. Rocket Soc. 21 (1951) 163–178.
[38] F. Nicoud, L. Benoit, C. Sensiau, T. Poinsot, AIAA J. 45 (2007) 426–441.
[39] L. Benoit, F. Nicoud, Int. J. Numer. Meth. Fluids 47 (2005) 849–855.
[40] A.D. Pierce, Acoustics: An Introduction to Its Physical Principles and Applications, McGraw Hill, New York, 1981.
[41] F. Silva, P. Guillemain, J. Kergomard, B. Mallaroni, A. Norris, J. Sound Vibrat. 322 (2009) 255–263.
[42] F. Nicoud, T. Poinsot, Combust. Flame 142 (2005) 153–159.
[43] R. Kaess, W. Polifke, T. Poinsot, N. Noiray, D. Durox, T. Schuller, S. Candel, in: Proc. of the Summer Program, Center for Turbulence Research, NASA AMES, Stanford University, USA, (2008) pp. 289–302.
[44] P. Wolf, G. Staffelbach, A. Roux, L. Gicquel, T. Poinsot, V. Moureau, C. R. Acad. Sci. Méc. 337 (2009) 385–394.
[45] M. Heckl, M. Howe, J. Sound Vibrat. 305 (2007) 672–688.
[46] D. Zhao, Combust. Flame 159 (2012) 2126–2137.